A&A manuscript no.
(will be inserted by hand later)

Your thesaurus codes are:
08 (08.01.1; 08.01.3; 08.13.2; 08.16.4; 08.23.2)

ASTRONOMY
AND
ASTROPHYSICS
20.5.1996

Spectral analyses of late–type WC central stars of planetary nebulae ⋆

U. Leuenhagen[1], **W.-R. Hamann**[2], **and C.S. Jeffery**[3]

[1] Institut für Astronomie und Astrophysik der Universität Kiel, D-24098 Kiel, Germany
[2] Lehrstuhl Astrophysik der Universität Potsdam, Postfach 601553, D-14415 Potsdam, Germany
[3] Dept of Physics and Astronomy, University of St Andrews, North Haugh, St. Andrews, Fife KY16 9SS, Scotland
e-mail (U.L.): leuenhagen@astrophysik.uni-kiel.de

Received date; accepted date

Abstract. The optical spectra of the seven late–type Wolf–Rayet central stars NGC 40 ([WC8]), BD+30°3639 ([WC9]), He 2–99 ([WC9]), CPD−56°8032, He 2–113, M 4–18 and K 2–16 (all [WC11]) are analyzed by means of spherically expanding model atmospheres. The NLTE simulations account for the elements helium, carbon and oxygen. As main results effective temperature T_*, element abundances and final velocity of the wind v_∞ are determined for each star. Assuming distances or luminosities for the objects, also the stellar radii and the mass–loss rates can be fixed. The values of T_* and v_∞ are found to be correlated with the spectral subtype ([WC8]: 78 kK, 1000 km s^{-1}; [WC9]: 47 – 49 kK, 700 – 900 km s^{-1}; [WC11]: 30 – 32 kK, 200 – 350 km s^{-1}). The obtained carbon–to–helium ratios are about unity (by mass), and the oxygen abundances are between 4 and 10 % (mass fractions). Stellar hydrogen abundances are below the limit of save detection in all cases (typically ≤ 2 % by mass); however in one star (He 2–113) we find a weak indication for the presence of hydrogen. Furthermore the occurrence of nitrogen lines in two of the stars (He 2–113, K 2–16) is discussed qualitatively. The results of these analyses put empirical constraints for the evolutionary status of WC–type central stars as post–AGB objects and provide input for modeling their planetary nebulae.

Key words: Stars: abundances – Stars: atmospheres – Stars: mass loss – Stars: AGB and post–AGB – Stars: Wolf–Rayet

1. Introduction

WC–type central stars of planetary nebula (WC–CSPN or [WC] according to van der Hucht et al. 1981) are characterized by an emission line spectrum of helium, carbon and oxygen. These emission lines are broadened due to the rapid wind velocities. Some features are P–Cygni shaped. In some late–type [WC] stars even hydrogen, nitrogen and heavier elements like silicon, aluminium, neon or iron are detectable. The separation in early– and late–type [WC] objects was established on observational grounds. Using the classification criteria of van der Hucht et al. (1981), Méndez & Niëmela (1982) and Hu & Bibo (1990), the known sample of galactic WC central stars covers mainly the subtypes [WC2] to [WC4] (early–type [WC] or [WCE]) and [WC8] to [WC12] (late–type [WC] or [WCL]). Only three stars of the intermediate subtypes [WC5] to [WC7] have been found until now (cf. Acker et al. 1995, Hamann 1995). The present paper is focussed on the late–type WC central stars.

In the recent past the Kiel group extended its spectral analyses from hot Population I Wolf–Rayet stars to the coolest WR–type objects, namely the late–type WC central stars. A pilot study was carried out for the [WC12] stellar spectrum of V 348 Sgr (Leuenhagen & Hamann 1994, hereafter Paper I). In this work we present the results of the analyses of seven further members of the subclass [WCL]. The model calculations used were originally developed for Pop. I WR–stars and are described in several publications (e.g. Hamann 1985, 1986, 1987, Hamann & Wessolowski 1990, Hamann et al. 1992, Koesterke et al. 1992a, Koesterke et al. 1992b). The numerical treatment of a [WCL] object is the same as for massive WR–stars. In both cases the radiation transfer must be examined in a spherically expanding atmosphere under non–LTE conditions. The only differences exist in lower values for the temperature, the mass–loss rate and the expansion velocity.

Section 2 contains general information about the program stars. The basic data of the observations are given in Sect. 3, the model calculations and atomic data are described in Sect. 4. The spectral fits and resulting parameters for the objects can

Send offprint requests to: U. Leuenhagen

⋆ Partly based on observations obtained at the German–Spanish Astronomical Center, Calar Alto, Spain, at the Anglo–Australian–Observatory, Australia, and at the European–Southern–Observatory, La Silla, Chile

Table 1. Alias names for the analyzed objects.

used here	subtype	PN G	Perek & Kohoutek (1967)	van der Hucht et al. (1981)	IRAS-positions	others
NGC 40	[WC8]	120.0+09.8	PK 120+9°1	[WR1]	00102 +7214	HD 826
He 2–99	[WC9]	309.0−04.2	PK 309−4°1	[WR14]	13487−6608	LSS 3169
BD+30°3639	[WC9]	064.7+05.0	PK 64+5°1	[WR31]	19327+3024	HD 184738, He 2–438
CPD−56°8032	[WC11]	332.9−09.9		[WR19]	17047−5650	He 3–1333
M 4–18	[WC11]	146.7+07.6	PK 146+7°1	[WR7]	04215+6000	
He 2–113	[WC11]	321.0+03.9	PK 321+3°1	[WR17]	14562−5406	LSS 3299, He 3–1044
K 2–16	[WC11]	352.9+11.4	PK 352+11°2		16416−2758	

be found in Sect. 5 and Sect. 6 contains some comments on the results, remarks about other spectral features and a discussion of the evolutionary status of the [WCL] objects. Final conclusions are drawn in Sect. 7.

2. The program stars

Six of the seven program stars are well–observed, both at optical and infrared wavelengths. The analysis of the infrared spectrum provided information about the composition and also about the evolution of the circumstellar dust shell of WC central stars (e.g. Aitken et al. 1980, Aitken & Roche 1984, Pottasch 1987, Siebenmorgen et al. 1994). Only K 2–16 has not been analyzed in any sense before. Up to now the evolutionary status of the [WCL] stars is described either as a transition phase between Asymptotic Giant Branch (AGB) and PN–stage (Le Bertre et al. 1989, van der Veen et al. 1989), or as a post–AGB object just suffering a final thermal pulse (Rao 1987). Compendious comparisons of the late–type WC–CSPN CPD−56°8032, He 2–113, M 4–18 and V 348 Sgr have been presented by Webster & Glass (1974) and Rao (1987). Note that the designation of the planetary nebula serves as alias names for the central star as well, and vice versa (Table 1).

2.1. NGC 40 (PN G 120.0+09.8)

NGC 40 was discovered by Fleming in 1912 and studied already by Wright (1913) and Paddock (1915). The central star ($V = 11\overset{\mathrm{m}}{.}58$, Tylenda et al. 1991) serves as prototype of the spectral subtype [WC8] (Hiltner & Schildt 1966). The planetary nebula is well extended, its diameter is 48″ (Clegg et al. 1983), a halo is visible up to 60″, and filaments reach distances of 70 – 100″. UV spectra (IUE) of the central star were analyzed by Bianchi & Grewing (1987). They estimated its interstellar reddening as $E_{B-V} = 0\overset{\mathrm{m}}{.}5$ and its distance as about 1 kpc (from comparison with the reddening and distance of three neighboring stars). The effective temperature of the central star was assessed to 30 – 35 kK using Stoy or Zanstra methods (Köppen & Tarafdar 1978, Harman & Seaton 1966, Preite-Martinez & Pottasch 1983). Bianchi (1992) used the models of expanding pure helium atmospheres by Wessolowski et al. (1988) and Schmutz et al. (1989) to estimate the effective temperature at 90 kK but mentioned an alternative possible solution at 33 kK. Most recent observations of Balick et al. (1995) show line profile variations (e.g. of C III 5696 Å) on a time scale of hours (cf. Sect. 6.1).

2.2. He 2–99 (PN G 309.0−04.2)

He 2–99 was catalogued by Henize in 1964. Kaler et al. (1989) published a fundamental atlas of identifications for the UV and optical spectrum of the $13\overset{\mathrm{m}}{.}8$ object. The authors claimed that in the case of carbon the ions C I to C V are visible simultaneously. In the view of low–resolution IUE spectra and a multitude of blends this statement does not seem to be very reliable. The analysis of the nebula (15″ in diameter) provided Zanstra and Stoy temperatures ($T_Z = 26$ kK and $T_S = 27$ kK, respectively), a reddening of $c = 0.9 \pm 0.2$ (corresponding to $E_{B-V} = 0\overset{\mathrm{m}}{.}65 \pm 0\overset{\mathrm{m}}{.}14$) and a Shklovsky distance of 2.4 kpc. The final velocity could be derived from the broadening of the emission lines (UV: 1000 – 2000 km s^{-1}, optical: 700 – 1000 km s^{-1}). Furthermore Kaler et al. estimated the abundance ratio of carbon to helium to 0.3 (particle numbers). Preite-Martinez et al. (1991) found an even higher temperature of $T_S = 41.5$ kK using the energy balance method.

2.3. BD+30°3639 (PN G 064.7+05.0)

Campbell (1893) discovered the emission line star BD+30°3639 and classified the spectrum as WR type. The object is also known as “Campbell’s star”. A brightness of $V = 10\overset{\mathrm{m}}{.}1$ is given by van der Hucht et al. (1981). The diameter of the planetary nebula can be resolved (5″). During the century since its discovery there have been many publications concerning BD+30°3639. Some of them yielded controversial results e.g. for the effective temperature of the central star or for the distance. Harman & Seaton (1966) determined a temperature of 46 kK, but they used an erroneously large Hβ flux (cf. O’Dell & Terzian 1970). Pottasch et al. (1978) found T_Z(H I) = 31 kK while declaring their result for the He II Zanstra temperature (T_Z(He II) = 64 kK) as unplausible. From the nebular He I emission Köppen & Tarafdar (1978) estimated a temperature of T_Z(He I) = 34 kK. Distance estimates scatter between 0.7 and 3.7 kpc. Leaving aside any statistical methods the most reliable values are those of Masson (1989) and Hajian et al. (1993), 2.8 and 2.68 kpc, respectively. Both values result from measurements of the increasing angular diameter of the planetary

nebula and the radial velocity of the nebula matter (Doppler shift of the nebula lines). Since the increase of the diameter is small, the error bars are considerably large (Masson: +4.7 kpc −1.2 kpc, Hajian et al. : ±0.81 kpc). One uncertainty of this method is given by the possibility, that the secular growth of the nebula might not entirely due to the motion of matter. Using the same technique but newest radio observations from the VLA Kawamura & Masson (1995) determine a distance of 1.5±0.4 kpc. Following Pwa et al. (1986) the final velocity of the wind of BD+30°3639 amounts to 790±50 km s^{-1} and the reddening is $E_{B-V} = 0\overset{m}{.}24$ (analysis of the absorption dip at 2200 Å). Siebenmorgen et al. (1994) presented an analysis of the infrared spectrum of BD+30°3639.

A comparison between the spectra of BD+30°3639 and the Pop. I Wolf–Rayet star HD 164270 (subtype WC9) was published by Smith & Aller (1971). While these authors mentioned systematic differences between CSPN and Pop. I objects (the CSPN should have weaker and narrower emissions), Méndez et al. (1991) also looked at the [WC9] object He 2–99 (see Sect. 2.2) and concluded that the stellar spectra of WR–CSPN and Pop. I WR stars of the same subtype are in principle undistinguishable.

Méndez et al. (1991) and Kaler et al. (1989) emphasized the similarity between the spectra of BD+30°3639 and He 2–99 (both subtype [WC9]). The only difference exists in slightly broader emission lines in the case of He 2–99. Comparing our spectra of these two objects we come to the same conclusion while adding the remark that the degree of ionization is a little bit higher in He 2–99 (somewhat smaller C II but stronger C IV emission lines).

2.4. CPD−56°8032 (PN G 332.9−09.9)

The object CPD−56°8032 was mentioned first by Bidelman et al. (1968) and Cowley & Hiltner (1969). It was classified as cool Wolf–Rayet star. Later Henize (1976) recognized that CPD−56°8032 is a central star of a planetary nebula. The magnitude of the central star is $m_V = 11\overset{m}{.}5$ (Tylenda et al. 1991) which is corrected for the brightness of the nearly pointlike nebula (1″.3 diameter, Roche et al. 1986). Aitken et al. (1980) determined a Zanstra temperature of $T_Z = 26$ kK. Using a relation between dust temperature and nebula radius Rao et al. (1990) gave an assessment for the distance (2.36 kpc). Also the reddening of CPD−56°8032 (interstellar: $E_{B-V} = 0\overset{m}{.}4$; amorphous carbon grains: $E_{B-V} = 0\overset{m}{.}25$ to $0\overset{m}{.}3$) was examined by Rao et al. . Following Pollacco et al. (1992) and Lawson & Jones (1995) CPD−56°8032 exhibits a weak RCrB–type variability ($\Delta V = 1^m - 1\overset{m}{.}5$). The latter authors mentioned also a 125 d oscillation at maximum light which they take as an indication for a binarity of CPD−56°8032.

2.5. He 2–113 (PN G 321.0+03.9)

Henize (1967) mentioned that the object #113 of his new (second) catalogue did not show a typical nebula spectrum. At that time He 2–113 was carefully classified as "possible" planetary nebula. The visual brightness of this pointlike source is $12\overset{m}{.}28$ (corrected for the nebula contamination, Tylenda et al. 1991). A Zanstra temperature of $T_Z = 29$ kK has been determined by Aitken et al. (1980). Le Bertre et al. (1989) derived a kinematic distance of 3.5 kpc and published photometric data for the UBVJHKLM bands. A reddening of $E_{B-V} = 1\overset{m}{.}05$ results from analyzing the Balmer decrement (Rao 1987).

2.6. M 4–18 (PN G 146.7+07.6)

In the case of M 4–18, discovered by Minkowski in 1959, the planetary nebula can be resolved (4″ diameter). A nebula corrected visual brightness of 14^m is given by Shaw & Kaler (1985). Goodrich & Dahari (1985) published a spectroscopic study of this object. The authors used the Stoy energy–balance method to determine an effective temperature of $T_S = 22$ kK for the central star. An interstellar reddening of $E_{B-V} = 0\overset{m}{.}9$ was derived from the Balmer decrement. No photometric variability could be detected. Furthermore Goodrich & Dahari mentioned an anomalous C IV 1550 Å absorption feature which seems to be extremely pressure broadened. Other [WC11] objects do not show this peculiarity. Assuming Cudworth's (1974) distance scale a statistical distance of 3.5 kpc was found.

2.7. K 2–16 (PN G 352.9+11.4)

In 1977 Kohoutek mentioned a new planetary nebula named K 2–16. The nebula has a diameter of 23″ and the visual brightness of the central star amounts to $12\overset{m}{.}8$ (Tylenda et al. 1991). Preite-Martinez et al. (1991) determined a Stoy temperature of $T_S = 19.6$ kK for this object (caution: in that paper K 2–16 is misspelled as "He 2-16"). This object shows a very close relationship to the [WC12] object V 348 Sgr. The properties of V 348 Sgr have already been analyzed (Paper I), together with a detailed description of the spectrum (Leuenhagen et al. 1994, hereafter Paper II). The most puzzling result of the spectral analysis of V 348 Sgr is that hydrogen and nitrogen are present in the wind along with a large amount of carbon. These results were corroborated by an independent LTE analysis of the absorption spectrum of V 348 Sgr (Jeffery 1995a).

3. The observations

Three of the program stars (He 2–99, CPD−56°8032 and He 2–113) are located in the southern sky. The observation of He 2–99 was carried out by U. Wessolowski on the ESO 3.6m Telescope at La Silla with the EFOSC spectrograph (échelle mode, spectral resolution 2.7 Å). The data for CPD−56°8032 and He 2–113 were collected by one of us (C.S.J.) using the 3.9m Anglo Australian Telescope (AAT) combined with an échelle spectrograph. These observations provide spectra of very high quality (0.7 Å resolution). The spectra of NGC 40, BD+30°3639, M 4–18 and K 2–16 were taken at Calar Alto, Spain, by W.-R.H. and L. Koesterke (1991 run) and by W.-R.H. and U. Wessolowski (1993 run) employing the Boller & Chivens spectrograph at the 2.2m telescope. The spectral resolution of

the Calar Alto spectra is again 2.7 Å. Table 2 summarizes the observations. The planetary nebulae of NGC 40, He 2–99 and K 2–16 are extended enough to allow the subtraction of the nebula background from the stellar spectrum during the process of data reduction.

Table 2. List of observations. Spectral ranges which have been observed twice or more are coadded. Because of the strong Hα nebula emission the red part of the spectrum of BD+30°3639 had to be observed several times.

Object	Date	Exp. time (sec)	Res. (Å)	Wavelength (Å)
NGC 40	July 6, 93	300	2.7	3450-4800
	June 29, 91	900	2.7	4550-6050
	June 28, 91	900	2.7	5900-7400
He 2–99	Febr. 14, 92	480	2.7	3800-9000
BD+30°3639	July 5, 93	480	2.7	3450-4800
	July 4, 93	700	2.7	4550-5900
	July 7, 93	82	2.7	5800-7200
	July 7, 93	40	2.7	5800-7200
	July 7, 93	60	2.7	5800-7200
	July 7, 93	180	2.7	5800-7200
CPD−56°8032	July 20, 89	2500	0.7	4050-4900
	July 21, 89	3595	0.7	4050-4900
He 2–113	July 21, 89	3601	0.7	4050-4900
	July 21, 89	3600	0.7	4050-4900
M 4–18	July 7, 93	1800	2.7	3450-4800
	July 12, 93	1800	2.7	4600-5950
K 2–16	July 6, 93	900	2.7	3450-4800
	July 10, 93	600	2.7	4600-5950
	July 7, 93	900	2.7	5800-7200

Beside the nebular emissions the dominating emission features in all spectra are those of He I, He II, C II – C IV and O II – O V. In the high quality spectra of CPD−56°8032 and He 2–113 also lines of P III (1, 3; multiplet numbers refering to Moore 1959), Mg II (4, 10), Al III (3), Si III (2, 9), and Si IV (1, 5, 6 and 7) can be detected. Only the profiles of He I, C IV, O II, Si III and Si IV lines show a blue shifted P–Cygni absorption feature. In the spectra of He 2–113, K 2–16 and probably M 4–18 also lines of singly and doubly ionized nitrogen are visible.

The similarity between the [WC9] objects BD+30°3639 and He 2–99 is already mentioned in Sect. 2.3. Within the sample of program stars there is another pair, namely CPD−56°8032 and He 2–113 (both [WC11]), whose spectra appear like twins (cf. Figs. 4 and 5). For the classification of the subtype only the carbon lines are taken into account. Hence it is remarkable that nearly all visible features (including O II, P III, Mg II, Al III, Si III and Si IV) are present in both spectra. The very few differences belong to slightly broader and stronger lines in CPD−56°8032 (higher final velocity of the wind and slightly enhanced density) and the presence of nitrogen (and possibly hydrogen, see Sect. 5.3) only in He 2–113. Note that the spectrum of M 4–18 (Fig. 6) is also very similar to the described pair, although the resemblance appears less striking due to the lower resolution of the data.

In Table 3 the image numbers of the IUE observations used in Sect. 5.2 are listed. Except K 2–16 all spectra were obtained as extracted data (data type “MELO”) from NDADS. In the case of multiple observation of one object the data have been merged. The observations of the variable object CPD−56°8032 were taken at maximum light. Most recent data of K 2–16 were obtained by K. Werner and kindly put at our disposal.

Table 3. List of IUE images.

Object	Image
NGC 40	SWP: 42187, 43240, 43241, 46380
	LWP: 20967, 21867
He 2–99	SWP: 28420, 28463
	LWP: 8321
BD+30°3639	SWP: 4923, 41867, 41868
	LWP: 9945, 20637
CPD−56°8032	SWP: 8947
	LWP: 7700
He 2–113	SWP: 8950, 42315
	LWP: 21075
M 4–18	SWP: 9659, 42313
	LWP: 8401, 8402, 21064
K 2–16	SWP: 55421
	LWP: 31223

4. The model calculations

The model calculations are based on the assumptions of homogeneity and stationarity. The atmospheres is supposed to be spherical. The velocity field is parametrized by the well–kown “β–law” using $\beta = 1.0$. The final velocity is a free parameter which can be easily determined by measuring the blueshift of observed P–Cygni profiles. Assuming a mass–loss rate the density stratification then follows from the equation of continuity. Further free parameters are the effective temperature T_*, the stellar radius R_* (luminosity: $L = 4\pi R_*^2\, \sigma T_*^4$) and the chemical composition.

The radiation transfer is solved separately for continuum and line frequencies. Neglecting the effects of moving matter (Doppler–shifts) the continuum transfer equation is treated with the momentum equations and variable Eddington factors. But undoubtedly the line radiation transfer must account for the expansion velocities. The transfer equation is transformed into the co–moving frame for that purpose (“CMF” technique by Mihalas et al. 1975). The equations of statistical equilibrium, augmented by the radiative equilibrium constraint, provide the non–LTE population numbers and the temperature stratification. In order to solve both systems of equations simultaneously (radiation transfer and statistical equilibrium) we make use of the Accelerated Lambda Iteration (ALI) technique.

Finally the synthetic spectrum is determined by performing a "formal solution" of the transfer equation in the observers frame. Within this procedure any combined levels can be split into substates. Frequency redistribution by electron scattering is taken into account in the formal solution.

Table 4. Number of NLTE levels of the model atom as applied for the different subtypes

	He			C				
subtype	I	II	III	I	II	III	IV	V
[WC8]	17	16	1	2	32	40	19	1
[WC9]	17	16	1	2	32	40	19	1
[WC11]	17	16	1	2	32	40	5	1

	O						
subtype	I	II	III	IV	V	VI	VII
[WC8]	–	3	33	25	18	15	1
[WC9]	3	30	33	25	2	–	–
[WC11]	3	30	3	1	–	–	–

Depending on the considered spectral subclass, the model atoms are adjusted to the specific requirements. E.g. the [WC8] star NGC 40 exhibits emission lines of O VI. Therefore, when modeling the [WC8] type spectra an extended oxygen model atom (O III to O VII) is taken into account. Since no O II lines are visible, this ion is represented only by three levels. In contrast, [WC11] type spectra show no emission of C IV and no lines of oxygen ions higher than O II. Consequently, the detailed model atoms of carbon and oxygen can be restricted to C II, C III and O II in that case. Table 4 gives the number of non–LTE levels per ion as applied for different spectral subtypes.

In general, we use the helium and carbon model atoms described in Hamann et al. (1992) and Paper I. The oxygen ions O I – O IV have been prepared for these analyses. The atomic data for O V, O VI and O VII are taken from Koesterke et al. (in prep.). For the detailed model ions of O II, O III and O IV all energy states up to the principle quantum number 5 are considered. Within the spin systems the angular momentum substates of n = 4 and n = 5 are each combined to a mean level. We use different sources for the level energies, namely Wenåker (1990, O II), Pettersson (1982, O III), Bashkin & Stoner (1975, O IV) and Opacity Project (O I, O II, O V, O VI, O VII). All f–values and data for radiative ionization were obtained from the Opacity Project.

One difference to the description of the carbon model atom in Paper I concerns the treatment of the "stabilizing lines" from so–called autoionization levels of C II and C III (doubly excited states with energies higher than the ionization limit of the ground state). For both ions we now consider 26 such levels which are assumed to be in LTE to the ground state of the next higher ion. In Paper I all stabilizing transitions from these LTE levels into states below the ionization energy are treated as normal lines, i.e. only Doppler broadening is considered and the rate equations are solved with an individual line radiation field calculated with the CMF technique. In the present work we distinguish between two categories of stabilizing lines, depending on the nature of the upper (autoionizing) level. Remember that the autoionization process is a spontaneous, radiationless transition which underlies selection rules (see also Sect. 6.3). For example all quartet states of C II above the ionization limit are not "allowed" to autoionize because of the conservation of the spin quantum number. Hence the lifetimes of these states might be not much shorter than those of bound levels, although they have positive energy. Consequently, stabilizing transitions from such levels lead to "normal" spectral lines (see e.g. multiplet C II (50) in Fig.13) with usual profiles. On the contrary, the probability of an "allowed" autoionization process is typically $10^{14}\,s^{-1}$. Due to this very short lifetime, the associated stabilizing lines are extremely broadened by radiative damping and can not be recognized in the spectrum. In contrast to Paper I lines of this kind are now treated as optically thin, i.e. the transition rates are calculated with the continuum radiation field, while the former category is treated like "normal"line transitions in the radiation transfer.

Table 5. Number of levels and transitions which are available in our model atom. Note that its actual complexity depends on the considered spectral subtype (see Table 4). The quoted "LTE" levels are all autoionizing states. Line transitions termed "LTE" refer to the stabilizing lines from autoionizing states.

Ion	levels		transitions			
	NLTE	LTE	exact NLTE	thin NLTE	exact LTE	thin LTE
(1)	(2)	(3)	(4)	(5)	(6)	(7)
H I	10	-	45	-	-	-
H II	1	-	-	-	-	-
He I	17	-	55	81	-	-
He II	16	-	120	-	-	-
He III	1	-	-	-	-	-
C I	2	-	1	-	-	-
C II	32	26	147	349	153	-
C III	40	26	222	558	106	191
C IV	19	-	171	55	-	-
C V	1	-	-	-	-	-
O I	3	-	3	3	-	-
O II	30	-	103	332	-	-
O III	33	-	528	408	-	-
O IV	25	-	300	211	-	-
O V	18	-	153	106	-	-
O VI	15	-	105	19	-	-
O VII	1	-	-	-	-	-

Table 5 shows how detailed our model ions are. The numbers of non–LTE and LTE levels can be found in Columns 2 and 3. Column 4 gives the number of lines for which the radiative

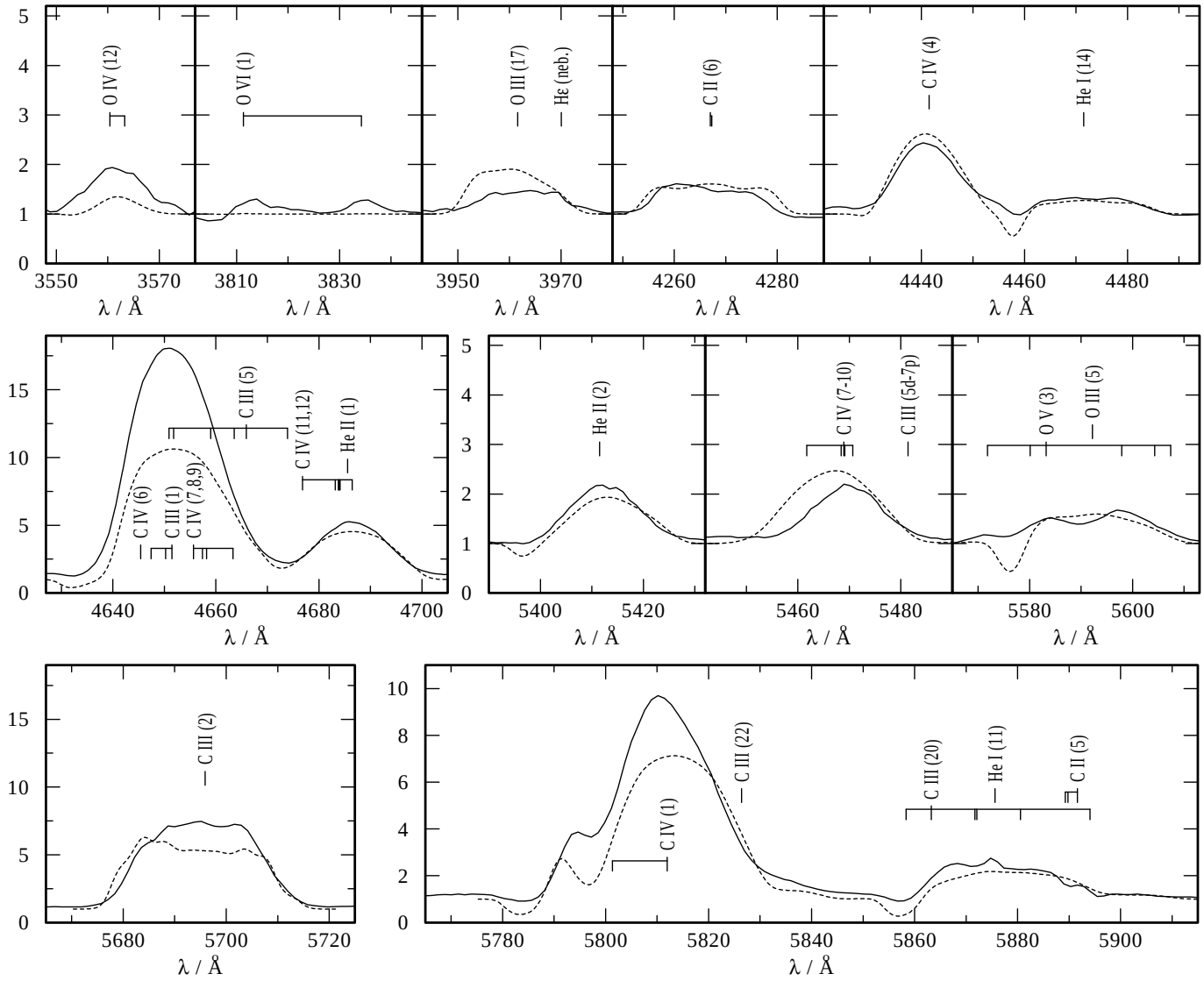

Fig. 1. Observations (solid line) and synthetic spectra (dashed line) of **NGC 40** (subtype [WC8]). Model parameters are described in Sect. 5. The synthetic profiles are convolved with a Gaussian of 2.7 Å (FWHM).

transfer is fully treated. Radiative rates of those lines with very small f–value (mainly forbidden lines) are evaluated with the continuum intensity (optically thin approximation, Column 5). Columns 6 and 7 refer to stabilizing lines. The former denotes the number of fully treated lines, the latter the number of transitions which are assumed to be optically thin.

For the search of an upper limit for the stellar hydrogen abundance energy levels of neutral and ionized hydrogen have been added to the model atom of the corresponding subtype (H I: 10 levels, H II: 1 level). The atomic data of hydrogen are taken from Hamann et al. (1991).

5. Results

The spectral analyses are based on an iterative fit procedure in order to reproduce the line strengths and profiles of different elements and ionization stages. Due to lack of suitable UV spectra, the comparison between synthetic spectra and observations is restricted to optical line transitions. The ratio of line strengths of He I to He II or C II to C III is very sensitive to variations in the effective temperature enabling a determination of this parameter with an error of only ± 1000 K. Concerning the mass–loss rate the emergent spectra will be clearly affected if $\dot{M}$ is changed by 0.1 dex. If temperature and mass–loss rate are increased simultaneously over a small range the effects may cancel because both parameters have opposite influences on the ionization balance. The element abundances for helium and carbon can be fixed with an error of $\pm 5\%$ (fraction of total mass). For the oxygen abundance the uncertainty is $\pm 2\%$.

One basic property of our model atmospheres is that models with the same ratio $R_*(v_\infty/\dot{M})^{2/3}$ (v_∞ in units of 2500 km/s and $\dot{M}$ in units of $10^{-4}\,M_\odot$/yr) — so–called "transformed ra-

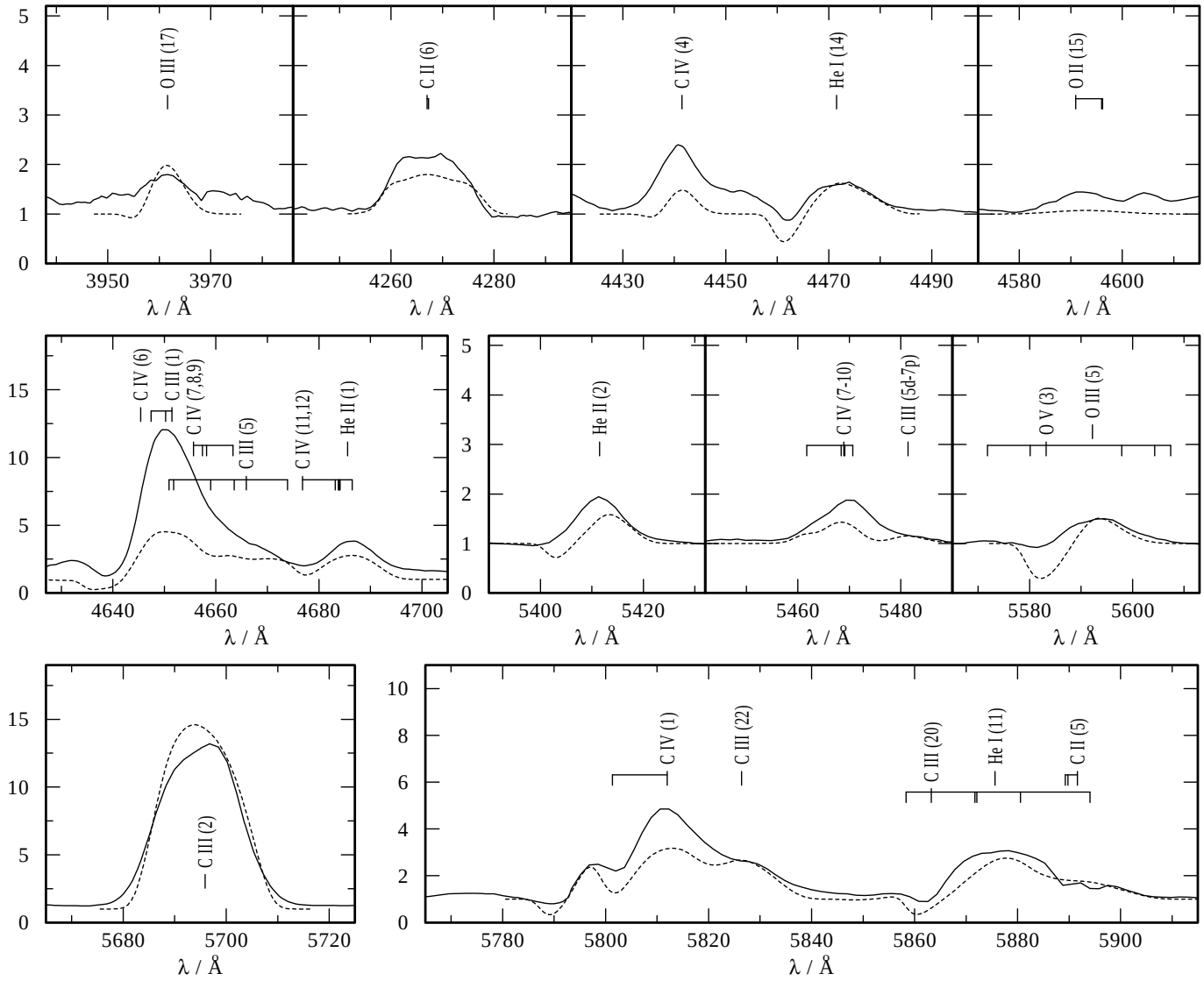

Fig. 2. Observations (solid line) and synthetic spectra (dashed line) of **He 2–99** (subtype [WC9]). Model parameters are described in Sect. 5. The synthetic profiles are convolved with a Gaussian of 2.7 Å (FWHM).

dius R_t") — exhibit almost identical emergent spectra (Schmutz et al. 1989, Hamann et al. 1992). This fact simplifies the fit procedure because there is one parameter less to vary. Having fixed the effective temperature, the element abundances, the final velocity and the transformed radius, in the next step the reddening is verified by comparing the model continuum flux with calibrated IUE spectra (low resolution mode). Simultaneously the dilution factor R_*^2/d^2 is determined. Assuming a luminosity or a distance, e.g. from the sources mentioned in Sect. 2, the stellar radius can be specified. Now the mass-loss rate follows from the definition of the transformed radius.

In Table 6 the parameters for each of the program stars are given. All values within the vertical bars depend on the distance adopted ($R_* \sim d$, $\dot{M} \sim d^{3/2}$, $L \sim d^2$). In the case of K 2–16 the luminosity instead of the distance is assumed.

5.1. Line fits

In Figs. 1 to 7 the observations and synthetic spectra of some important lines are illustrated. Note that the wavelength scale of Figs. 4 to 7 is twice that of Figs. 1 to 3. The wavelengths of the identification marks and the designations of the multiplets refer to Moore (1959, 1970).

The main goal of the fit procedure for each star is to find a combination of effective temperature, wind density (defined by mass–loss rate and stellar radius) and element abundances which reproduce the observed spectrum in an acceptable way. For the comparison between synthetic spectra and observations we select preferably unblended lines of different elements and ions. The sample contains the multiplets He I 4471 Å, He I 5876 Å, He II 5412 Å, the classification lines of carbon (C II 4267 Å, C III 5696 Å, C IV 5801, 5811 Å), C IV 4442 Å, C IV

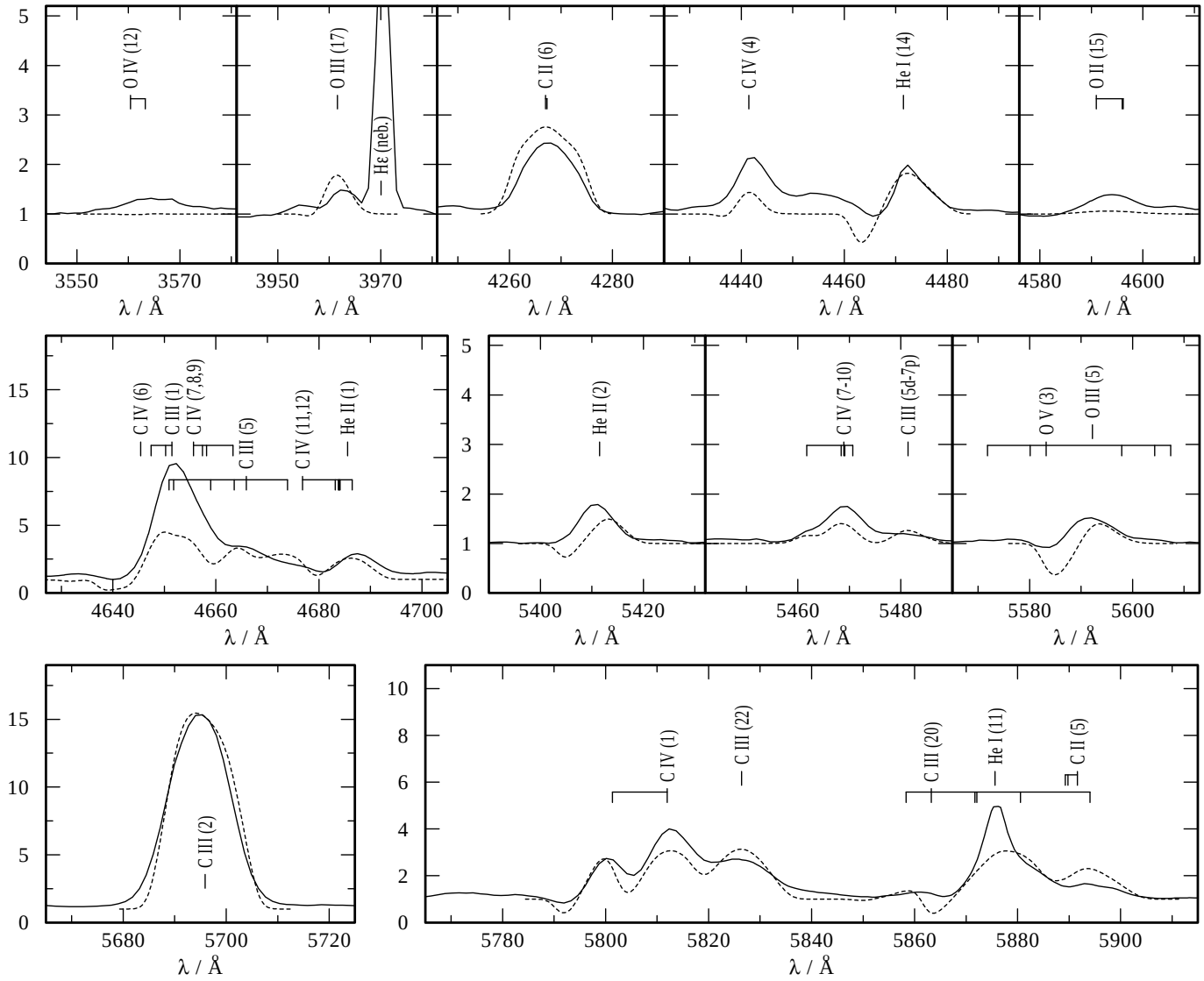

Fig. 3. Observations (solid line) and synthetic spectra (dashed line) of **BD+30°3639** (subtype [WC9]). Model parameters are described in Sect. 5. The synthetic profiles are convolved with a Gaussian of 2.7 Å (FWHM).

5470 Å, O II 4590 Å, O III 3960 Å, O IV 3560 Å, O V 5590 Å (blend with O III) and O VI 3811, 3834 Å plus some weaker transitions in the neighborhood of these lines. No features of C IV and O III – O VI are visible in the [WC11] objects. Of special interest is the wavelength region 4610 – 4720 Å for two reasons. Firstly, the appearance of this part of the spectrum is very different for various subtypes. Whereas the [WC8] and [WC9] objects exhibit a huge blend of He II, C III and C IV emissions the [WC11] spectra show much smaller and narrower lines of He I, He II (weak), C II, C III and O II. Secondly, an increase of the continuum level is visible between 4610 Å and 4640 Å in the [WC11]–type spectra (see Sect. 6.3).

In the following paragraphs some remarks on individual objects are made:

– *NGC 40* (Fig. 1): This spectrum is reproduced convincingly. Solely the weak O VI multiplet at 3811, 3834 Å and O IV 3560 Å cannot be modeled. The observed feature at 5590 Å exhibits a multiplet structure and must be therefore formed mainly by O V. The synthetic profile, however, is dominated by O III (see also Sect. 6.1). C III 5696 Å is very sensitive to variations of the temperature or the mass–loss rate. A decrease of $\dot{M}$ by 0.1 dex causes a doubling of the line strength, an increase of the temperature from 78 kK to 80 kK will halve the peak height of this line. It is impossible to fit C III 5696 Å and the blend complex at 4650 Å simultaneously. At the center wavelength of He I 5876 Å a residual nebula emission is visible.

– *He 2–99* (Fig. 2) and *BD+30°3639* (Fig. 3): Apart from the different line shapes both spectra exhibit the same set of stellar emission features but the detailed comparison reveals the differences mentioned above. He 2–99 shows stronger, broader lines (reflecting the higher final velocity v_∞ and the

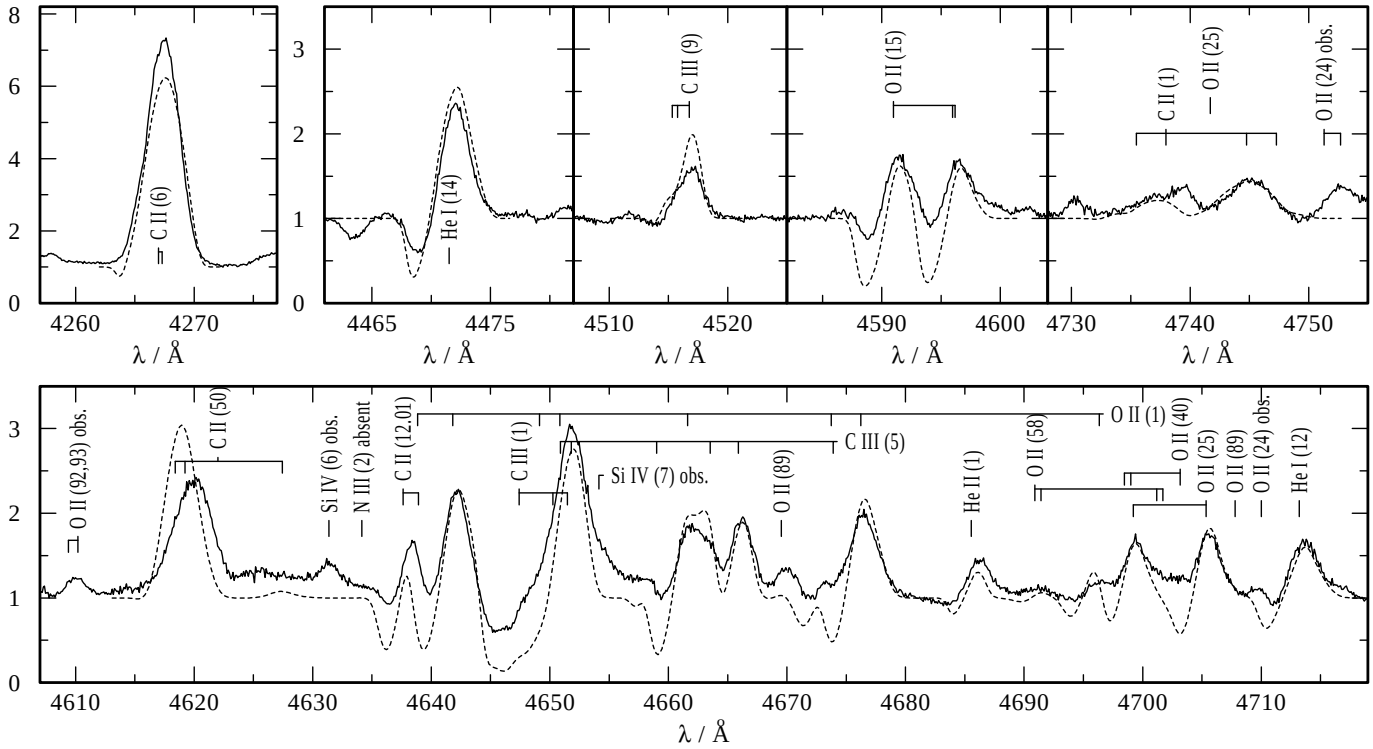

Fig. 4. Observations (solid line) and synthetic spectra (dashed line) of **CPD−56°8032** (subtype [WC11]). Model parameters are described in Sect. 5. The synthetic profiles are convoluted by a Gaussian of 0.7 Å (FWHM). Identifications augmented by "obs." refer to lines which are not accounted for in the models. In contradiction to He 2–113 (Fig. 5) the N III emission at 4634 Å is absent.

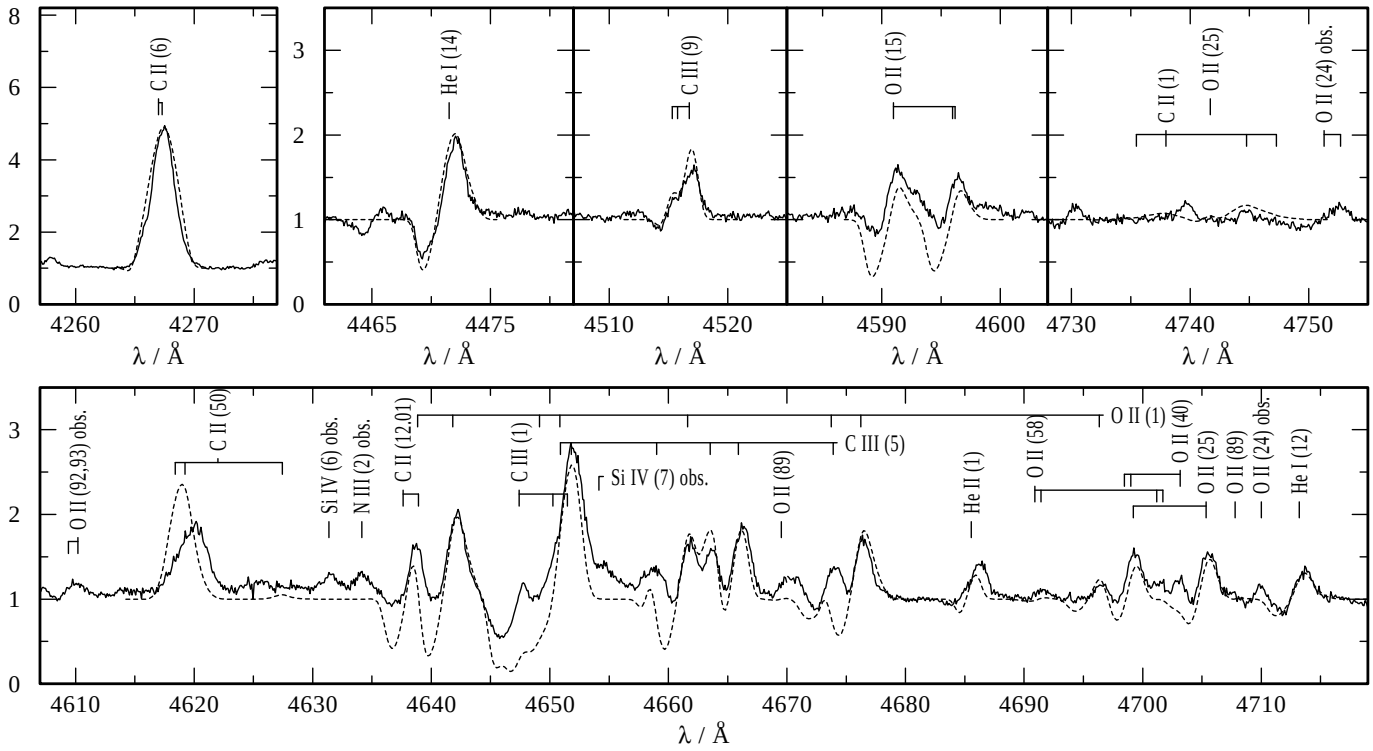

Fig. 5. Observations (solid line) and synthetic spectra (dashed line) of **He 2–113** (subtype [WC11]). Model parameters are described in Sect. 5. The synthetic profiles are convoluted by a Gaussian of 0.7 Å (FWHM). Identifications augmented by "obs." refer to lines which are not accounted for in the models.

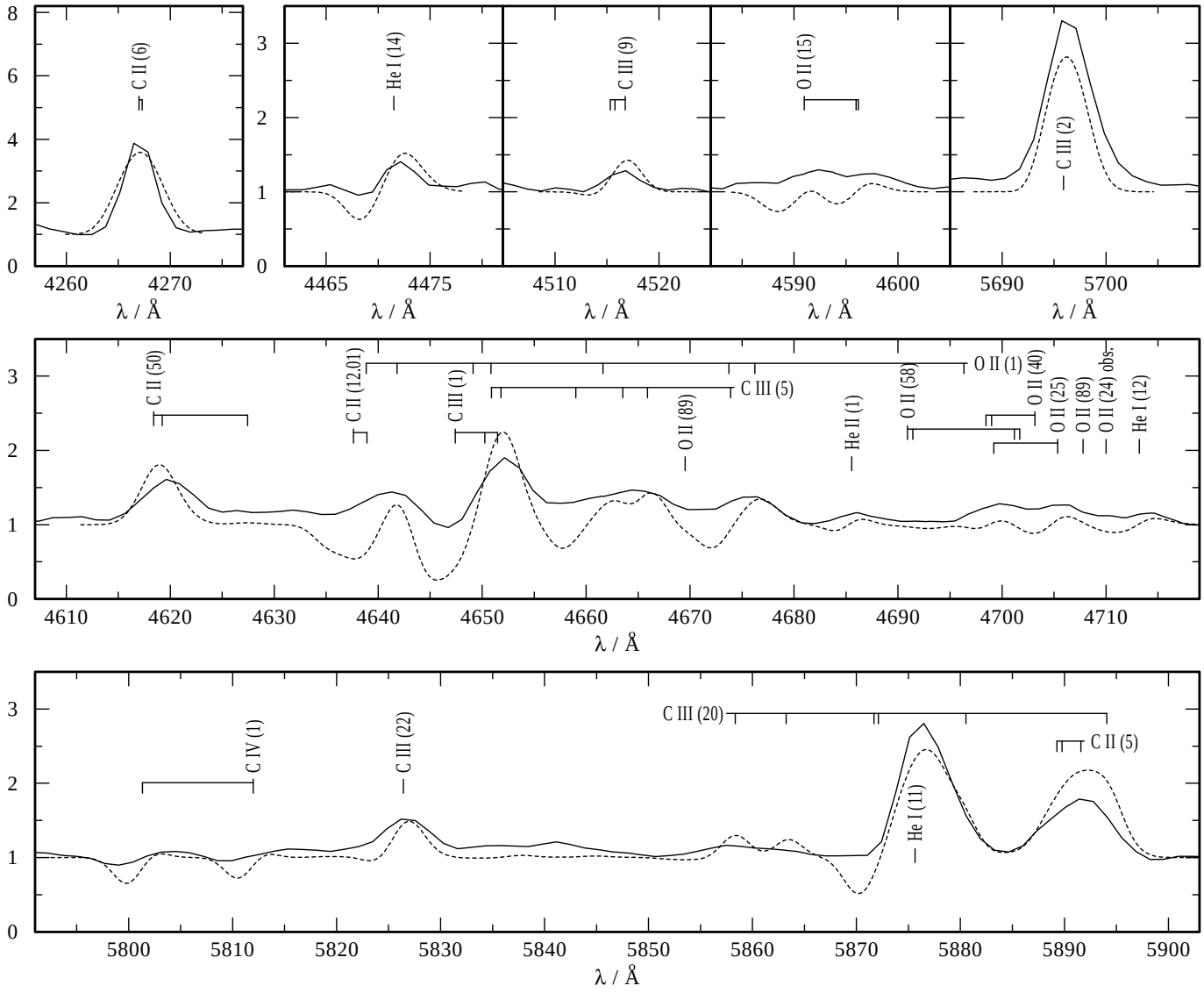

Fig. 6. Observations (solid line) and synthetic spectra (dashed line) of **M 4–18** (subtype [WC11]). Model parameters are described in Sect. 5. The synthetic profiles are convoluted by a Gaussian of 2.7 Å (FWHM). Identifications augmented by "obs." refer to lines which are not accounted for in the models.

higher density of the wind) and a slightly higher degree of ionization (higher effective temperature). Furthermore the oxygen lines seem to be stronger compared to helium and carbon features in He 2–99.

The quality of the spectral fit is acceptable, even though the lines of O II (4590 Å) and O IV (3560 Å, BD+30°3639 only) are not reproduced well. The line strength ratio of the carbon classification lines (C II 4267 Å, C III 5696 Å and C IV 5801, 5811 Å) is different for the two [WC9] objects. In the case of BD+30°3639 this ratio can be fitted satisfactorily, but the model atmosphere for He 2–99 shows simultaneously a too strong C III line and too weak emissions for C II and C IV. The He I lines of BD+30°3639 are superimposed by sharp emission cores of nebula origin (especially He I 5876 Å). Concerning the 4650 Å complex the same remarks as for NGC 40 apply here. Contrary to NGC 40 the feature at 5590 Å is of singlet structure and must be therefore attributed to O III.

– *CPD−56°8032* (Fig. 4) and *He 2–113* (Fig. 5): Only spectra of the blue range are available to us. Concerning the C IV line at 5801, 5811 Å this might be no disadvantage, because no emission is expected (see also M 4–18 and K 2–16). Instead of C III 5696 Å we use the transition at 4516 Å and a component of the multiplet C III (5) at 4666 Å as reference lines. The helium features are also useful temperature indicators. Even though the absorption parts of the P–Cygni profiles are overestimated, the spectral fits of these two [WC11] objects are reasonable.
– *M 4–18* (Fig. 6): Apart from the poor resolution the spectrum of M 4–18 is very similar to CPD−56°8032 and

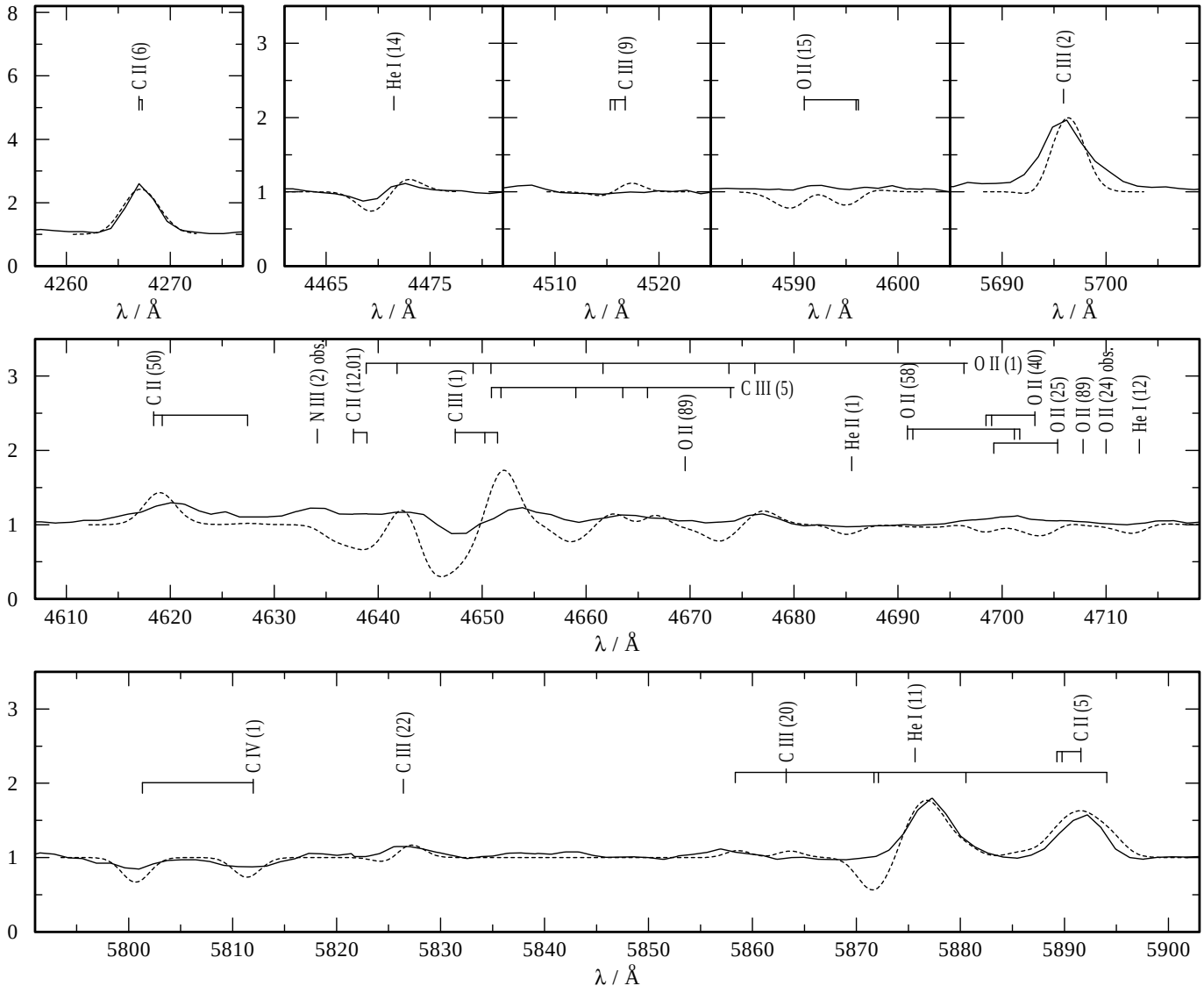

Fig. 7. Observations (solid line) and synthetic spectra (dashed line) of **K 2–16** (subtype [WC11]). Model parameters are described in Sect. 5. The synthetic profiles are convoluted by a Gaussian of 2.7 Å (FWHM). Identifications augmented by "obs." refer to lines which are not accounted for in the models.

He 2–113. The observed line widths of M 4–18, which are broader than those of the objects mentioned in the last paragraph, are not only caused by the instrumental profile, but also by a higher final velocity of the wind. The theoretical C III 5696 Å line is slightly too weak but if the temperature is increased by only 1000 K the synthetic profile will surpass the observation already. In correspondence with the observations the components of the multiplet C IV 5801, 5811 Å appear as weak absorption dips.

– *K 2–16* (Fig. 7): In this spectrum no "strong" lines are visible. Even the classification lines of carbon and the line complex at 4650 Å are relatively weak. For most of the identification marks in Fig. 7 are in fact no corresponding features in the observed spectrum. The weakness or absence of the emissions can be simulated by a model atmosphere with a low wind density. All helium and carbon lines are fitted well, except the 4650 Å feature which is overestimated. Since no oxygen line can be identified definitely, only an upper limit for the oxygen abundance can be determined.

5.2. Continuum fits

The comparison of the model flux distributions — reddened with a standard law according to Seaton (1979) and Abbott et al. (1984) — with absolutely calibrated IUE data (see Table 3) yields a dilution factor R_*^2/d^2 for each object. Also the visual brightness is taken into account (calibration according to Heber et al. 1984). Assuming a distance this dilution factor defines a stellar radius and — using the relation for the transformed radius — the final choice of the mass–loss rate.

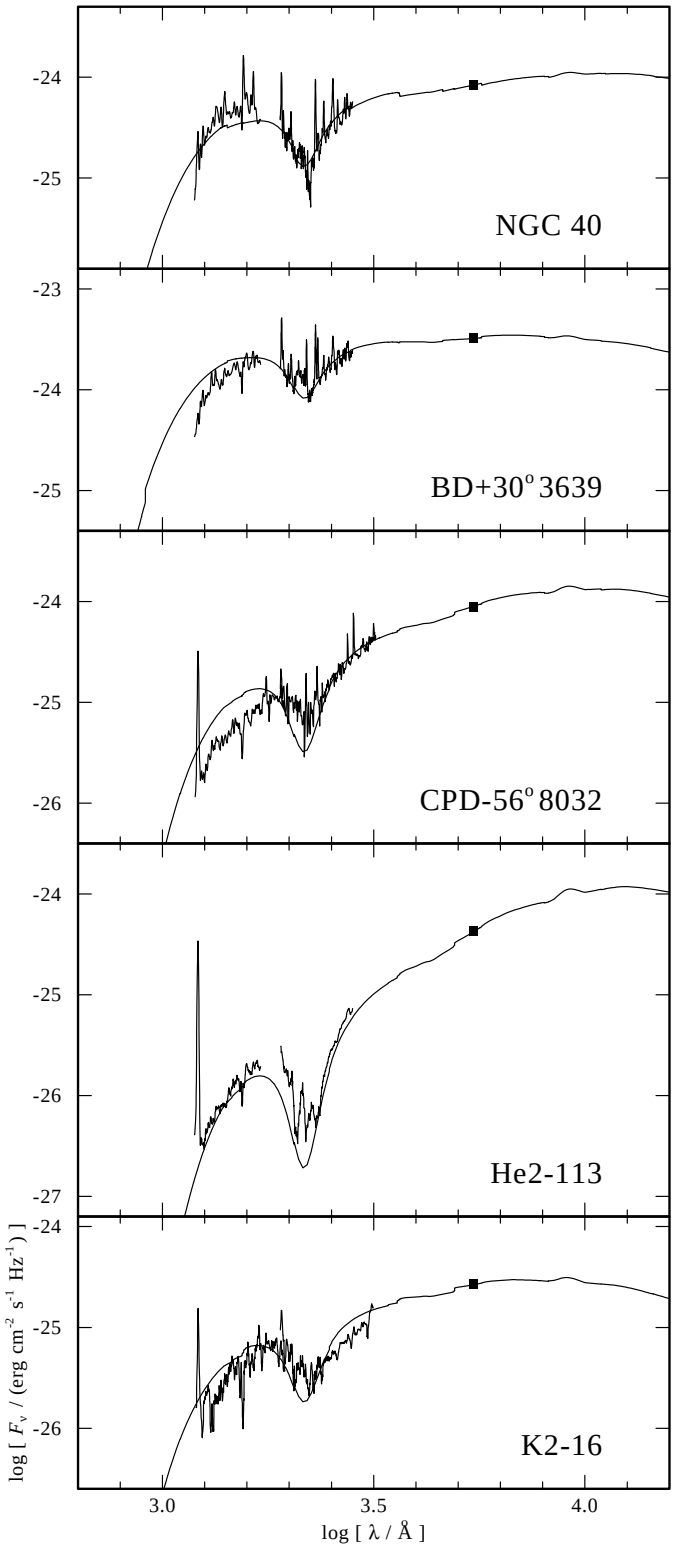

Fig. 8. Flux distribution of NGC 40, BD+30°3639, CPD−56°8032, He 2–113 and K 2–16. Plotted are calibrated IUE fluxes and the model fluxes of the atmospheres described in Sect. 5. In each diagram the filled square marks the observed visual brightness of the object. The model fluxes are reddened with $E_{B-V} = 0^m.45$ (NGC 40), $0^m.4$ (BD+30° 3639), $0^m.7$ (CPD−56°8032), $1^m.05$ (He 2–113) and $0^m.6$ (K 2–16), respectively.

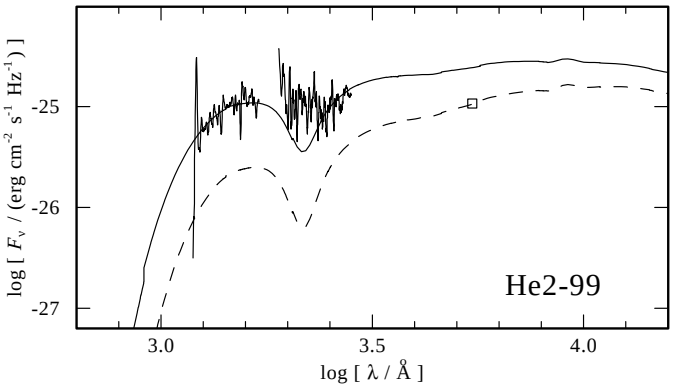

Fig. 9. Flux distribution of He 2–99. Plotted are calibrated IUE fluxes and the model continuum (parameters according Table 6). The dashed line shows the model continuum reddened with $E_{B-V} = 0^m.65$ and adjusted to the visual brightness $m_V = 13^m.8$ (open square) according to Kaler et al. (1989). We prefer a reddening of $E_{B-V} = 0^m.5$, which is represented by the solid line. The visual brightness of this model flux is $12^m.89$.

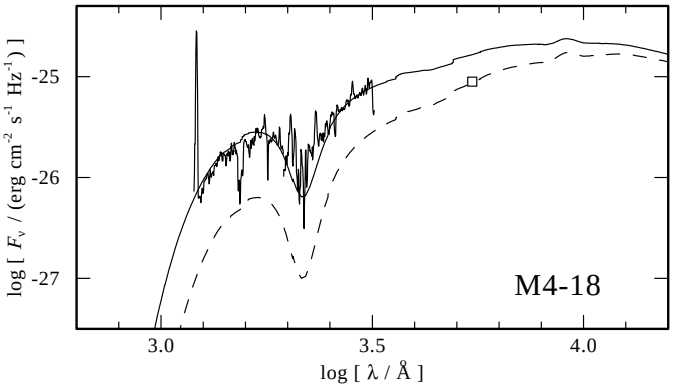

Fig. 10. Flux distribution of M 4–18. Plotted are calibrated IUE fluxes and model fluxes (see Table 6 for parameters). The dashed line represents the flux distribution reddened with $E_{B-V} = 0^m.9$ (Goodrich & Dahari 1985) and adjusted to the visual brightness $m_V = 14^m$ (Shaw & Kaler 1985, open square). In order to reproduce the IUE data more satisfactorily we use a reddening of $E_{B-V} = 0^m.7$. The so–adjusted model flux (solid line) has a visual brightness of $13^m.30$.

In Fig. 8 the continuum fits of five program stars are shown. Except BD+30°3639 ($E_{B-V} = 0^m.4$ instead of $0^m.24$) the values for reddening and visual brightness correspond to the sources given in Sect. 2. In the case of CPD−56°8032 the steepness of the flux contradicts the weakness of the absorption dip. The standard reddening law overestimates the extinction near 2200 Å (cf. Jeffery 1995b). For K 2–16 a reddening of $E_{B-V} = 0^m.6$ is adopted. The observed absorption feature at 2200 Å seems to be shifted to longer wavelengths, which might be caused by a large amount of circumstellar carbon grains. Detailed studies on the extinction of K 2–16 are not yet known.

For two objects we prefer values for the extinction and angular radii based on UV fluxes alone. The data of Kaler et al. (1989) for extinction ($c = 0.9$ or $E_{B-V} = 0^m.65$) and visual

brightness ($m_V = 13\overset{m}{.}8$) fail to correspond with the ultraviolet measurements of He 2–99 (see Fig. 9). We adopt a reddening of $E_{B-V} = 0\overset{m}{.}5$ ($c = 0.69$) which fits the SWP slope, but overestimates the 2200 Å absorption. The corresponding visual magnitude is $12\overset{m}{.}89$. Since the Shklovsky distance depends on the reddening assumed, the value of Kaler et al. (2.4 kpc) must be scaled ($c = 0.69$ leads to 2.53 kpc).

The visual brightness of M 4–18 of $m_V = 14^m$ as given by Shaw & Kaler (1985, nebula corrected brightness) do not correspond to the IUE data as well (Fig. 10). This is probably caused by an overestimate of the nebula brightness. In this case we trust the uncorrected ultraviolet observations which are believed to be uncontaminated by the nebula. From our fit of the IUE spectra we find $E_{B-V} = 0\overset{m}{.}7$. The visual brightness of the so–adjusted model flux is $m_V = 13\overset{m}{.}30$.

5.3. Hydrogen abundance

The detection of stellar hydrogen in [WCL]–type spectra is a delicate procedure because several components are merging at Balmer wavelengths. The planetary nebula produces narrow pure emission lines whose strengths depend on the nebula properties. Additionally, stellar features of hydrogen (possibly) and singly ionized helium are located at these wavelengths. The abundance ratios between He, C and O given in Table 6 are derived from unblended lines. For checking the H–abundance, hydrogen is now added to the atmosphere leaving the He:C:O ratio unchanged.

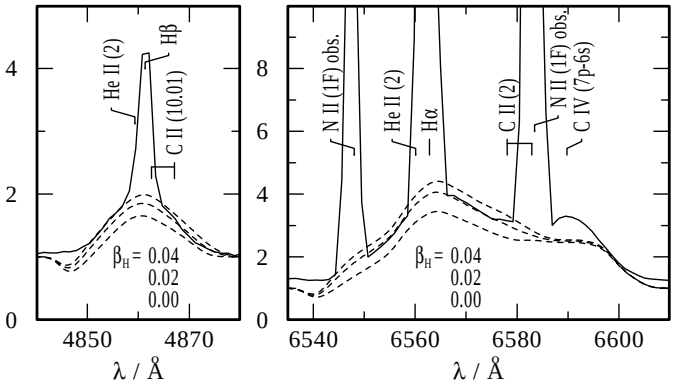

Fig. 11. Observed spectrum of **NGC 40** (solid lines) around He II 4860 Å/Hβ (left) and He II 6560 Å/Hα (right), compared with synthetic spectra for different hydrogen abundances (dashed lines). The labels denote the hydrogen mass fraction β_H of the model atmosphere. Other model parameters are as compiled in Table 6. The ratio β_{He}:β_C:β_O is kept constant for all values of β_H. The synthetic profiles are convolved with a Gaussian of 2.7 Å (FWHM).

In the case of the [WC8] and [WC9] subtypes the nebular lines can be distinguished easily from the stellar features due to the strong broadening of the latter (wind velocities 700-1000 km s^{-1}). On the other hand this effect would merge the stellar He II line with a possible hydrogen contribution, as their laboratory wavelengths are separated by only 124 km s^{-1} (Doppler units). Representative for these subtypes, Fig. 11 shows the observed and the synthetic spectrum around Hβ and Hα of NGC 40. Obviously the contribution of the hydrogen lines would be stronger than permitted by the observation if $\beta_H > 2\,\%$.

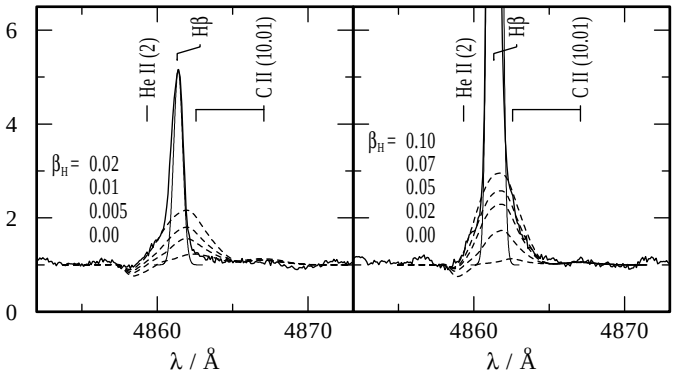

Fig. 12. Observed spectra (thick solid lines) of **CPD−56°8032** (left) and **He 2–113** (right) around He II 4860 Å/Hβ, compared with synthetic profiles for different hydrogen abundances (dashed lines). The labels denote the hydrogen mass fraction β_H. Other model parameters are as compiled in Table 6. The ratio β_{He}:β_C:β_O is kept constant for all values of β_H. The synthetic profiles are convolved with a Gaussian of 0.7 Å (FWHM). As an estimate for the expected instrumental broadening, a Gaussian with 0.7 Å FWHM and peak height of the corresponding Hβ nebular line is also plotted (thin solid lines).

The wind velocities in the [WC11] objects are smaller than in the earlier subtypes. Moreover, the He II emissions of [WC11] stars are weaker due to their lower effective temperature. Only in the high resolution spectra of CPD−56°8032 and He 2–113 the helium contribution becomes visible by additional emission at the blue wing of the nebular lines (see Fig. 12). In the case of M 4–18 (2.7 Å resolution) a possible stellar line is completely hidden behind the strong nebular Balmer emissions (not shown in the figures). The nebula of K 2–16 is well resolved. After subtraction of the nebula background, the Balmer lines are nearly removed (also not shown). Remarkable differences can be found between the spectra of CPD−56°8032 and He 2–113 (cf. Fig. 12). Since the blue wing of Hβ is contaminated by the He II transition we concentrate on the red wing. The line profile of CPD−56°8032 matches almost perfectly the expected instrumental broadening function (Gaussian of 0.7 Å FWHM, thin solid line). This leads to the sharp upper limit $\beta_H \leq 0.5\,\%$ for the hydrogen mass fraction. In the spectrum of He 2–113, however, the same profile shows an extended red wing which cannot be reproduced by the expected instrumental broadening profile (again a Gaussian of 0.7 Å FWHM, thin solid line). This part of the emission feature can be explained by a model atmosphere with $\beta_H = 7\,\%$.

Summarizing, stellar hydrogen is not detected definitely in any of our program stars, with the upper limits as compiled in Table 6. Thus the definite detection of hydrogen in the [WC12]–type spectrum of V 348 Sgr (4 % by mass, Paper I) remains un-

Table 6. Parameters of [WCL]–type central stars. In addition to the effective temperature T_* also the temperature $T_{2/3}$ referring to the radius R ($\tau_{\rm Ross} = 2/3$) is given. The definition of the transformed radius $R_{\rm t}$ is given in Sect. 5. The dilution factor R_*^2/d^2 is determined from the continuum fits (see Sect. 5.2). Note that all parameters within the vertical bars depend on the adopted distances (see Sect. 2 and 5.2). Due to the lack of information about the distance of K 2–16 the luminosity of this object is presumed (distance in brackets follows from $\log L/L_\odot = 3.7$). The element abundances are given in mass fractions ($\beta_{\rm He}+\beta_{\rm C}+\beta_{\rm O}$=100 %, except V 348 Sgr). In two cases the results for the upper limits of $\beta_{\rm H}$ are badly influenced by strong nebular lines (in brackets). Parameters of V 348 Sgr are improved results of Paper I.

						distance dependent results				chemical comp.			
	T_* [kK]	$T_{2/3}$ [kK]	v_∞ [km s^{-1}]	$R_{\rm t}$ [$R_\odot$]	$\log R_*^2/d^2$	d [kpc]	R_* [$R_\odot$]	$\log \dot{M}$ [$M_\odot$/yr]	$\log L$ [$L_\odot$]	$\beta_{\rm H}$ [%]	$\beta_{\rm He}$ [%]	$\beta_{\rm C}$ [%]	$\beta_{\rm O}$ [%]
NGC 40	78	46	1000	2.16	−22.26	1.00	0.33	−5.62	3.58	≤ 2	40	50	10
He 2–99	49	45	900	5.76	−22.12	2.53	0.97	−5.59	3.72	≤ 2	50	40	10
BD+30°3639	47	42	700	5.46	−21.10	2.68	3.32	−4.87	4.71	(≤ 7)	45	50	5
CPD−56°8032	32	30	240	7.92	−20.97	2.36	3.40	−5.57	4.06	≤ 0.5	42	50	8
M 4–18	31	30	350	13.69	−21.65	3.50	2.30	−6.01	3.67	(≤ 10)	46	50	4
He 2–113	30	29	200	12.99	−20.75	3.50	6.49	−5.54	4.51	≤ 7	44	50	6
K 2–16	30	29	300	20.88	−21.55	(3.43)	2.56	−6.36	3.70	≤ 1	45	50	5
V 348 Sgr	20	20	190	49.97	−21.00	(4.24)	5.75	−6.53	3.70	4	40	55	≤ 1

precedented for [WCL]-type central stars. However, the direct comparison of the spectra of CPD−56°8032 and He 2–113 suggests the presence of a few mass-percent hydrogen the case of He 2–113.

6. Discussion

6.1. Model parameters

In general the observed emission line spectra of cool Wolf–Rayet central stars (subtypes [WC8], [WC9] and [WC11]) can be reproduced by our model atmospheres. For most lines the predicted and observed strengths agree much better than within a factor of two.

However, notorious problems are encountered whenever more than two ionizing stages of the same element are visible in the spectrum, e.g. O III to O VI in NGC 40. Our models fail to reproduce the features of all observed ions simultaneously. Depending on the chosen model parameters, either the higher or the lower ions (or both) are underestimated (see O VI 3811, 3834 Å in Fig. 1 or O IV 3561 Å and O II 4590 Å in Fig. 3). One possible explanation of this effect is that the model assumption of homogeneity is not precisely fulfilled in these stellar winds. A local decrease of the density would favor the population of the higher ions. In the case of an inhomogeneous atmosphere the emergent spectrum gathers various contributions. The features of highly ionized matter originate form parts of lower density, while lines from lower ions form in denser volumes. Under these circumstances it is conceivable that the features of both lower and higher ions (e.g. O III and O VI) might appear in comparable strengths. Such spectra cannot be satisfactorily reproduced by a homogeneous model atmosphere. First explorations of these problems, which are also encountered with Pop. I Wolf-Rayet stars, are in progress.

In a recent publication, Balick et al. (1995) measured line profile variations in the spectrum of NGC 40. The authors reported about narrow features (emissions or absorptions) which firstly appear in the line center of e.g. C III 5696 Å and then move either to the blue or to the red edge of the line on time scales of hours. This phenomenon can be explained by "blobs" of denser or thinner matter which are accelerated in radial direction either towards the observer or away from him. The lifetime of these features (a few hours) is consistent with the crossing time of a mass element through the line formation region of our model atmospheres. These observations are the direct evidence for inhomogeneities in the wind of Wolf–Rayet stars.

An effective temperature of 90 kK for the object NGC 40 was published by Bianchi (1992) using pure helium model atmospheres of Wessolowski et al. (1988) and Schmutz et al. (1989). However, Bianchi mentioned a second possible solution at 33 kK. Taking into account that a strong cooling effect occurs if carbon is considered (Hamann et al. 1992), Bianchi's lower value might correspond to the present result (78 kK).

The spectra of He 2–99 and BD+30°3639 are rather similar. Consequently, the obtained values for effective temperatures and *transformed* radii almost agree. Nevertheless, the stellar radii and the mass–loss rates differ considerably. To a minor part, this is due to the slightly higher final wind velocity which we find for He 2–99 than for BD+30°3639, in accordance with Méndez et al. (1991). More important, this demonstrates that the results for the stellar radius, mass–loss rate and luminosity obtained from our spectral analyses also depend on the assumed distances. The $d = 2.68$ kpc which we adopt for BD+30°3639 (Hajian et al. 1993) is based on the measured increase of the nebular's angular size and therefore rather reliable (cf. Sect. 2). On the contrary, the distance to He 2–99 is completely uncertain. Our adopted value (2.53 kpc) stems only from the Shklovsky method. Now, these two stars have a very different appearent visual brightness, He 2–99 being more than $3^{\rm m}$ fainter than BD+30°3639. Adopting the quoted, rather similar values for the distances, this leads to very different absolute magnitudes, and thus finally to the large differences in the resulting stellar radii, mass–loss rates and luminosities of the two [WC9] objects (cf. Table 6). Alternatively, one might assume that both stars

have similar absolute parameters, implying that the Shklovsky distance for He 2–99 is largely in error.

Within the sample of seven [WCL] objects a strong correlation between effective temperature and subtype can be found. This is not a trivial result because the ionization balances depend not only on the effective temperature, but also on the density in the wind (more precisely, the *transformed radius*). Some scatter in this correlation is reflected by the different effective temperatures for the four [WC11] stars, which per definition have similar line strength ratios C II / C III.

Another interrelation concerns the final velocity of the stellar wind and the spectral subtype (or effective temperature). Neglecting the variance within one subtype, v_∞ is correlated with T_*. Even the [WC12] object V 348 Sgr fits in that correlation (stellar parameters from Paper I). As shown by Pauldrach et al. (1988) this behavior can be principally explained by radiative driven winds. Especially for central stars with optically thin winds (like IC 418 or even the helium rich objects A 30 and A 78) the model calculations of Pauldrach et al. predict the right scale for final velocities and mass–loss rates. But not so for the WCL–type central stars, which show much smaller wind velocities but considerably stronger mass–loss rates compared to the above mentioned species of PN's. Thus the radiation–driven wind models accelerate too little matter at too high velocities. This conclusion resembles the situation for massive stars, as the radiation-driven wind theory in its present form can account for, e.g., O, Of and B stars, but not for the Pop. I Wolf-Rayet objects.

6.2. Zanstra temperatures of the model atmospheres

The results for the effective temperature of the analyzed [WCL] stars are considerably higher than the values from nebula based methods (Zanstra or Stoy temperatures). This discrepancy can be attributed to deficiencies of the latter methods. The Zanstra– and Stoy–methods both infer the ionizing radiation from the strengths of nebula lines. Assuming a blackbody radiation field the estimated flux then defines an effective temperature. Beside the question of whether the planetary nebula is optically thick or not, the comparison with a blackbody flux will underestimate the temperature of the central star. Indeed the continuum flux of the model atmospheres shows a pronounced flux deficit shortward of 911 Å due to continuous absorption by C II or C III ions. The relevant parameter for determining a Zanstra temperature is the ratio $\pi\, F_\nu^{\rm ref} \,/\, \int_{\nu_0}^{\infty} (\pi\, F_\nu / h\,\nu)\; d\nu$, where F_ν is the continuous flux distribution and $F_\nu^{\rm ref}$ is the flux at a reference wavelength. The integral sums up all the ionizing photons for one ion, e.g. H I or He I. If a blackbody flux is assumed ($F_\nu = B_\nu$) this ratio depends only on the temperature. A comparison of the model flux ratio with the corresponding ratio of a Planck function yields Zanstra temperatures predicted from the model atmospheres (Table 7). The reference wavelengths for $T_{\rm Z}$ (H I), $T_{\rm Z}$ (He I) and $T_{\rm Z}$ (He II) are 4860 Å, 5876 Å and 4686 Å, respectively.

In the atmosphere of a hot star, the emergent flux is effectively blocked by ionization edges in the UV. In order to preserve the bolometric flux, the blocked energy escapes as visual and IR radiation. Moreover, stellar winds produce an excess of radiation towards longer wavelengths. This IR excess can already start in the visual spectrum when the wind is very dense. The low H I and He I Zanstra temperatures of the [WC8] and [WC9] models are mainly induced by the compensating enhancement of visual flux and the "IR excess" starting in the visual. Additionally, strong C III edges at 259 Å and 300 Å decimate the He II ionizing flux. In the case of the [WC11] objects the model flux at optical wavelengths (e.g. the above mentioned reference wavelengths) roughly corresponds to the blackbody flux for T_*. Here, the differences between T_* and the Zanstra temperatures are due to the deficit of ionizing flux only. Particularly the low values for $T_{\rm Z}$ (He I) are caused by a strong C II edge at 508 Å blocking the He I ionizing flux.

Table 7. Comparison of the model flux with a blackbody flux (Zanstra temperatures predicted from the model atmospheres).

object	subtype	T_* [kK]	$T_{\rm Z}$ (H I) [kK]	$T_{\rm Z}$ (He I) [kK]	$T_{\rm Z}$ (He II) [kK]
NGC 40	[WC8]	78	48	47	17
He 2–99	[WC9]	49	42	33	15
BD+30°3639	[WC9]	47	40	13	11
CPD−56°8032	[WC11]	32	31	12	9
M 4–18	[WC11]	31	31	12	<9
He 2–113	[WC11]	30	31	12	<9
K 2–16	[WC11]	30	29	11	<9

6.3. Spectral peculiarities

The spectra of [WCL]–type objects show some peculiarities. One is the apparent enhancement of the continuum between 4610 Å and 4640 Å (see Fig. 13). This feature has been also mentioned in connection with the [WC12] object V 348 Sgr by Houziaux (1968) and in Paper II. The identification with the multiplet C II (50) as given in Paper II seems now to be questionable because our high quality spectra of CPD−56°8032 and He 2–113 show a further emission at 4620 Å which is very likely due to C II (50). Moreover, the wavelengths of C II (50) given by Moore (1970) do not match the position of the 4620 Å feature as exactly as in the case of all other lines. The modeled line profile of C II (50) — positioned at the Moore wavelengths — slightly surpasses the observed line strength but reproduces the line shape (see Figs. 4 to 7).

Both participating atomic levels of the transition C II (50) — $1s^2\,2s\,2p\,(^3P^o)\,3d\,^2F^o$ and $1s^2\,2s\,2p\,(^3P^o)\,4f\,^2G$ — have energies higher than the ionization energy of the C II ground state. Energetically they are able to autoionize, but the configuration of the inner electrons ($^3P^o$) does not harmonize with the ground state of C III (^1S). Hence, the probability of the autoionization process, which is radiationless, cannot be very high and the lifetimes of these doubly excited levels are comparable to those of bounded levels. This is supported by the observed profile of the 4620 Å feature (in [WC11]–type spectra) which is not extremely broadened by radiation damping

effects. The absence of this line in V 348 Sgr is due to the lower effective temperature of that [WC12] star (20 kK) which shows no C III emissions at all.

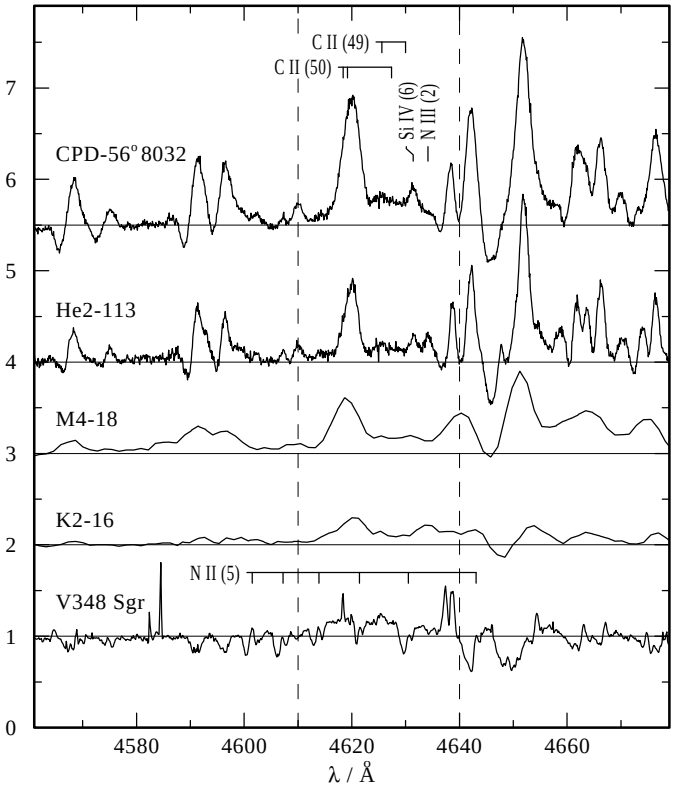

Fig. 13. Normalized spectra of [WC11] and [WC12] objects in the wavelength range 4560 – 4680 Å. Between 4610 Å and 4640 Å the continuum level seems to be enhanced ("emission bump"). The spectra of V 348 Sgr is taken from Paper II.

Along with the detailed presentation of the high resolution spectra of V 348 Sgr Paper II supplies a spectral atlas for extreme helium stars (EHe). The authors recognized that at the wavelengths of the 4610 to 4640 Å feature (centered near 4620 Å) in most of the EHe objects hotter than 14 kK an unusually broad absorption can be found. Only those EHe stars with weak or absent carbon spectra do not show this feature. Therefore the "emission bump" of the [WCL] stars and the broad absorption of the EHe's are probably caused by carbon, but the exact origin is still unclear.

Another spectral peculiarity concerns the presence of nitrogen. Some of the [WCL] objects exhibit N II or N III emissions, while others do not. However, due to the stronger broadening from higher wind velocities it is difficult to identify the weak nitrogen features in the subtypes [WC8] and [WC9]. Within the [WC11] group nitrogen can be clearly identified in He 2–113 and K 2–16. The detection of N II in M 4–18 is uncertain. In the spectrum of CPD−56°8032 nitrogen is definitely absent.

The detection of nitrogen in He 2–113 and the absence of this element in CPD−56°8032 is surprising, since these stars are almost twins according to other criteria (Figs. 4, 5 and 13). This might be discussed together with the hydrogen estimates (cf. Sect. 5.3). In the case of He 2–113 we found a weak indication for the presence of hydrogen (7 % by mass), while for CPD−56°8032 hydrogen is below 0.5 % definitely. Hence, in He 2–113 hydrogen might be present along with nitrogen, while both are absent in CPD−56°8032. Thus in He 2–113 material from former hydrogen-burning layers is still mixed into the present photosphere, while this material is lost entirely in the case of CPD−56°8032.

Within our sample of program stars, K 2–16 provides the strongest nitrogen lines (N II, not shown in the figures). In view of the weakness of all other lines the nitrogen abundance must be enhanced in this object compared to the others (analyses of the nitrogen lines in [WCL] objects are in progress). In this sense K 2–16 shows a close relationship to the [WC12]–type star V 348 Sgr. Refering to Paper I, V 348 Sgr exhibits not only a distinct nitrogen spectra but also stellar hydrogen lines with strong P–Cygni absorption edges. However, the hydrogen limit for K 2–16 is rather sharp (1% per mass), in contrast to V 348 Sgr and to the discussion in the preceding paragraph.

6.4. Status of evolution

Although some basic facts are established, the evolutionary status of [WCL] objects is still not understood in detail. The existence of a planetary nebula *per se* points to a post–AGB phase. The large fraction of processed matter in the stellar wind leads to the same conclusion. But what happens to these stars after leaving the asymptotic giant branch? Following a standard evolution scenario (H–burner), the mass–loss decreases and a hydrogen layer remains visible at the stellar surface. Due to several "dredge–ups" the atmospheric abundances of carbon and oxygen might be slightly enhanced, but far below the ratio $\beta_C/\beta_{He} > 1$ (mass fractions) found here. Alternatively, if the star leaves the AGB as a He–burner the evolution proceeds slower and the ongoing mass–loss perhaps removes the hydrogen–rich envelope. But again the predicted carbon fraction (cf. Blöcker 1995) would be much lower than we found empirically.

At the end of the AGB evolution several "thermal pulses" might intensify the mass–loss. The most interesting scenario regarding the [WCL] objects assumes that the departure from the AGB happens just before the next thermal pulse is scheduled. In this case the star can suffer a "late thermal pulse" while being already a central star or even almost a white dwarf. This leads to a repeated AGB excursion, connected with additional mass–loss ("born–again–scenario"). According to Blöcker (1993, 1995) such an evolutionary course — even multiple late thermal pulses are possible — would facilitate the complete removal or burning of hydrogen *and* helium, i.e. only a naked C/O core remains at the beginning of the White Dwarf cooling sequence.

Figure 14 illustrates the positions of the analyzed [WCL] objects in the HR–diagram together with evolutionary tracks from Blöcker (1993, 1995) and Paczyński (1970). Only tracks with one or more late thermal pulses are drawn because they represent the most plausible scenario. All objects are located within

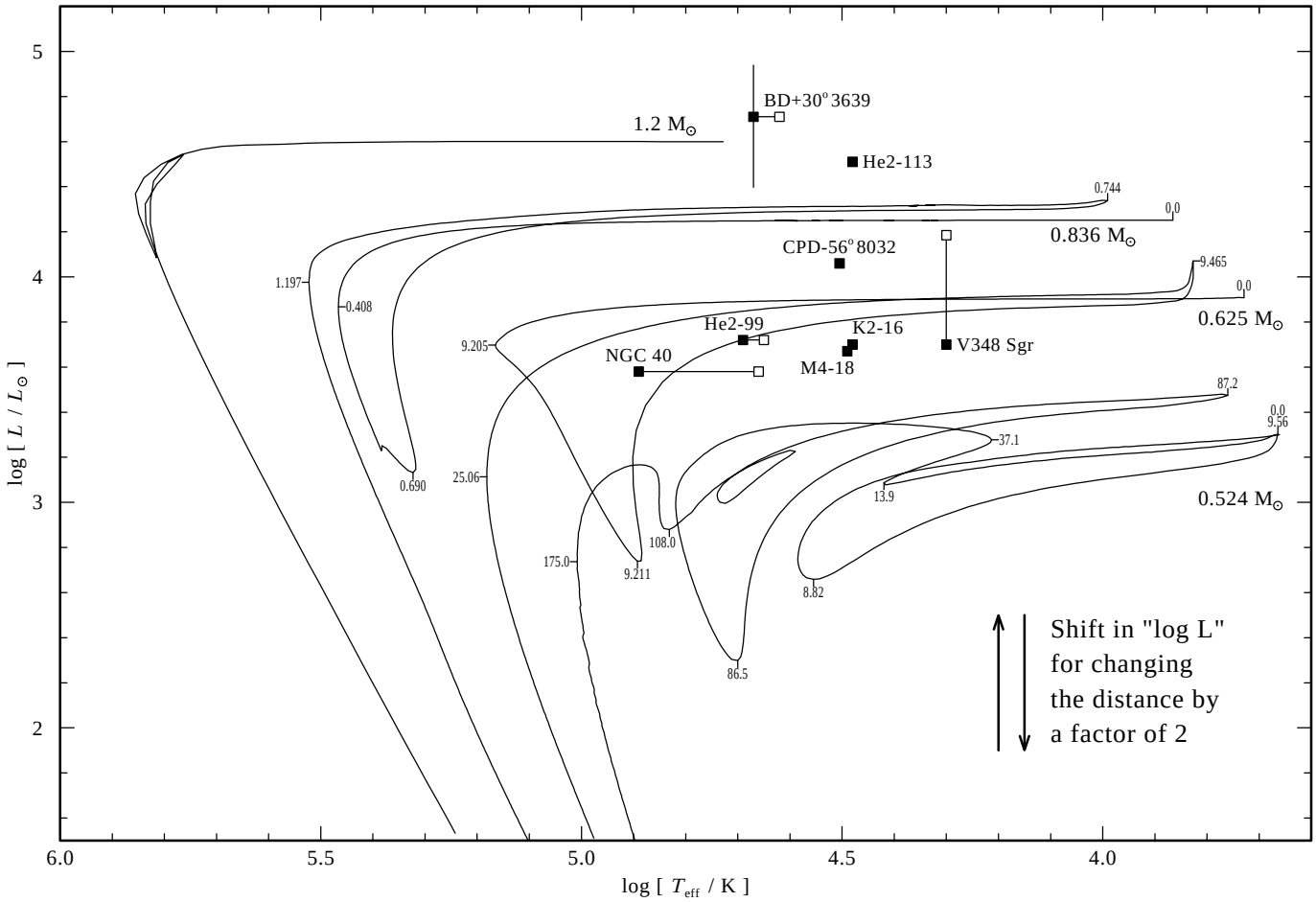

Fig. 14. HR–diagram with evolutionary tracks from Blöcker (1993, 1995) and Paczyński (1970). The tickmarks on the tracks denote the time (in 10^3 yr) since leaving the AGB. The filled squares give the positions of the analyzed [WCL] stars. For NGC 40, He 2–99 and BD+30°3639 the position with $T_{2/3}$ instead of T_* is marked too (open squares). The vertical line for BD+30°3639 represents the error bar of the distance according to Hajian et al. (1993). Note that the empirical luminosities depend on the adopted distances ($L \sim d^2$) which are unsure for some objects (see Sect. 2 and 5). The data for V 348 Sgr are taken from Paper I (filled square: presumed luminosity of $\log L/L_\odot = 3.7$, open square: alternative luminosity corresponding to $d = 8$ kpc as supposed by Schönberner 1986).

an area crossed by the evolutionary paths. The parameters of V 348 Sgr are from Paper I. The position of BD+30°3639 suggests a core mass higher than 1.2 $M_\odot$, but again we must emphasize that the exact position in the HRD depends on the adopted distance ($L \sim d^2$, see also the arrows in the lower right corner of Fig. 14). Adopting a distance of 1.5 kpc for BD+30°3639 (Kawamura & Masson 1995) the luminosity results to $\log L/L_\odot = 4.2$ which leads to a mass of roughly 0.8 $M_\odot$.

Refering to Blöcker (priv. comm.) the surface composition along the tracks shown in Fig. 14 is still dominated by helium until the "knee" at maximum temperature is reached. This fact is not consistent with our empirical abundances of the [WCL]'s which are located in the midst of the horizontal parts of the evolutionary tracks (central star phase). The visibility of remaining hydrogen or nitrogen in some of the analyzed objects can be probably explained by convective processes during a late thermal pulse (Iben et al. 1983).

Thus there remains the question how the hydrogen– and helium–rich layers can be removed by mass-loss or mixing. Is it possible that many late thermal pulses occur? Perhaps there is more mass–loss during a late pulse than expected. These questions are relevant for the evolutionary past of all hydrogen-deficient post–AGB stars (EHe, RCrB, [WCE], PG 1159, non–DA white dwarfs).

What is the future of [WCL] objects? A "normal" CSPN first evolves to higher temperatures. Later, after nuclear burning has terminated, the star follows the cooling track for White Dwarfs. In principle this evolution is conceivable for late–type WC central stars as well. In this case hotter counterparts must be identified. The comparison between the element abundances in [WCL] stars (this paper) and PG 1159 objects (as analyzed by Werner et al. 1991 or Dreizler et al. 1995) reveals a close similarity. Following these authors most of the analyzed PG 1159 stars, which suffer no mass–loss anymore, show an abundance ratio $\beta_C/\beta_{He} > 1$ as well. Compared to the [WCL]'s the oxy-

gen abundance of the much hotter PG 1159 stars seems to be increased (mostly $\beta_O = 10-20\%$ of the mass). This suggests that [WCL] stars are the progenitors of the PG 1159 objects. In support of this suggestion, some of the PG 1159 stars are surrounded by a faint nebula remnant. The possible evolution from [WCL] to PG 1159 would then inevitably pass through the parameter domain of the [WCE] objects, which are as hot as the PG 1159 stars but which still suffer strong mass–loss. Hamann & Koesterke (1993) and Koesterke & Hamann (1995) performed first analyses of these early–type WC–CSPN. Their results for the carbon–to–helium ratio ($\beta_C/\beta_{He} \approx 0.5$) seem to be slightly lower than the values typically found for [WCL] stars ($\beta_C/\beta_{He} \approx 1$). This would rule out the suggested evolution [WCL] $\rightarrow$ [WCE] $\rightarrow$ PG 1159. However, the significance of the still somewhat preliminary [WCE] analyses must be checked further. Due to the lack of intermediate subtypes — only three objects within [WC5] – [WC7] are found up to now — the possible evolution from [WCL] to [WCE] must pass these subtypes very fast.

7. Summary and conclusions

The detailed analyses of the optical spectra of seven late–type Wolf–Rayet central stars are presented, namely NGC 40 ([WC8]), BD+30°3639, He 2–99 (both [WC9]), CPD−56°8032, He 2–113, M 4–18 and K 2–16 (all [WC11]). The simulations of the expanding atmospheres are characterized by spherical symmetry, homogeneity, stationarity, ad–hoc velocity field, non–LTE conditions, self–consistent electron temperature (radiative equilibrium) and radiative transfer by co–moving frame technique. The model calculations account for the elements hydrogen, helium, carbon and oxygen.

The resulting effective temperatures of the program stars are found to correlate with the spectral subtype: 30 – 32 kK for [WC11], 47 – 49 kK for [WC9] and 78 kK for [WC8]. Also the final velocities of the wind (200 – 350 km s^{-1} for [WC11] and 1000 km s^{-1} for [WC8]) are correlated to the subtypes (or effective temperatures). The element abundances are — apart from small variations — similar for all analyzed central stars. With one exception the mass ratio of carbon to helium surpasses unity. The atmospheric abundance of oxygen reaches mass fractions of 4 – 10 %. The analyses of the Balmer lines provide restrictions for the hydrogen abundances. For NGC 40 and He 2–99 the upper limit for the mass fraction of hydrogen results to $\beta_H \leq 2\,\%$, for K 2–16 to $\beta_H \leq 1\,\%$. In one case (CPD−56°8032) we found a limit of $\beta_H \leq 0.5\,\%$. For the other stars any β_H above 10 % can be excluded. There are some relevant indications (extended emission at the red wing of the superimposed nebular Hβ) for a hydrogen abundance of $\beta_H = 7\,\%$ in the wind of He 2–113. For expanding stellar atmospheres, a spectral analysis alone yields the "transformed radius" which is defined by the ratio $R_*(v_\infty/\dot{M})^{2/3}$. Adopting distances for the individual objects, we then derive stellar radii, mass–loss rates and luminosities. These absolute quantities must be rescaled if a different distance is assumed.

The theoretical continuum fluxes for the program star models are available from the authors and may be used as input for nebula modeling instead of blackbody radiation.

The existence of an ordinary planetary nebula implies a post–AGB status of the late–type WC–CSPN. But due to the large portion of processed matter at the stellar surface a "normal" central star evolution must be rejected. Obviously the hydrogen–rich layer and also parts of the helium–rich layer have been removed, either by strong mass–loss or deep convective mixing. Both happens during "late thermal pulses" which lead to repeated post–AGB phases ("born–again–scenario"). In two of the spectra nitrogen is visible, which can be also explained by convective processes during a late thermal pulse. Nevertheless the analyzed abundances are similar to those of [WCE] and PG 1159 objects. Assuming an increasing temperature ([WCL] $\rightarrow$ [WCE]) and a decreasing mass–loss rate ([WCE] $\rightarrow$ PG 1159) these three groups might be evolutionary linked.

Acknowledgements. We thank Ulf Wessolowski and Lars Koesterke for their contribution collecting the observational data. Klaus Werner provided us with IUE data of K 2–16, all other IUE spectra we received via NDADS. The model calculations were performed on the CRAY supercomputers of the Rechenzentrum der Universität Kiel and the Konrad–Zuse–Zentrum für Informationstechnik Berlin (ZIB). U.L. acknowledges support from Deutsche Forschungsgemeinschaft under grant We 1312/10-1.

Note added in proof: The analysis of K2-16 was repeated with a better spectrum ($\sim$1 Å resolution) which we obtained in the meantime with the 3.5m telescope (TWIN spectrograph) at Calar Alto, Spain. The improved parameters obtained from the spectral fit are now: T_*=29 kK ($T_{2/3}$=28 kK), v_∞=180 km s^{-1} and R_t=23.54 $R_\odot$. Assuming a luminosity of $\log L/L_\odot$=3.7 stellar radius and mass–loss rate ($\log \dot{M}/[M_\odot\ \mathrm{yr}^{-1}]$) amount to 2.80 $R_\odot$ and -6.53, respectively. The element abundances remain unchanged, the oxygen abundance of 5 % (mass fraction) is confirmed.

References

Abbott D.C., Telesco C.M., Wolff S.C., 1984, Astrophys. J. 279, 225
Acker A., Górny S.K., Cuisinier F., 1995, Astron. Astrophys. (in press)
Aitken D.K., Barlow M.J., Roche P.F., Spenser P.M., 1980, Monthly Notices Roy. Astron. Soc. 192, 679
Aitken D.K., Roche P.F., 1984, Monthly Notices Roy. Astron. Soc. 208, 751
Balick B., Rodgers B., Hajian A., Terzian Y., Bianchi L., 1995, Astron. Astrophys. (in press)
Bashkin S., Stoner Jr. J.O., 1975, "Atomic Energy Levels and Grotrian Diagrams. Volume I. Hydrogen I - Phosphorus XV", North-Holland Publishing Company, Amsterdam
Bianchi L., 1992, Astron. Astrophys. 253, 447
Bianchi L., Grewing M., 1987, Astron. Astrophys. 181, 85
Bidelman W.P., Macconnell D.J., Bond H.E., 1968, Circ. Bureau Central Telegrammes N. 2089
Blöcker T., 1993, Acta Astron. 43, 305
Blöcker T., 1995, Astron. Astrophys. 299, 755
Campbell W.W., 1893, Publ. Astron. Soc. Pacific 5, 204
Clegg R., Seaton M., Peimbert M., Torres-Peimbert S., 1983, Monthly Notices Roy. Astron. Soc. 205,417
Cowley A.P., Hiltner W.A., 1969, Astron. Astrophys. 3, 372

Cudworth K.M., 1974, Astron. J. 79, 1384
Daub C.T., 1982, Astrophys. J. 260, 612
Dreizler S., Werner K., Heber U., 1995, in: White Dwarfs, Proc. of 9th European Workshop on White Dwarfs, D. Koester & K. Werner (eds.), Lecture Notes in Physics, Springer Verlag, p. 160
Goodrich R.W., Dahari O., 1985, Astrophys. J. 289, 342
Hajian A.R., Terzian Y., Bignell C., 1993, Astron. J. 106, 1965
Hamann W.-R., 1985, Astron. Astrophys. 148, 364
Hamann W.-R., 1986, Astron. Astrophys. 160, 347
Hamann W.-R., 1987, in: Numerical Radiative Transfer, ed. W. Kalkofen, Cambridge University Press, p. 35
Hamann W.-R., 1995, in: Proc. of the workshop *Planetary Nebulas with WR Type Nuclei* held on Ven, Astrophysics and Space Science (in press)
Hamann W.-R., Koesterke L., 1993, in: Planetary Nebulae, Proc. IAU Symp. 155, R. Weinberger & A. Acker (eds.), p. 87
Hamann W.-R., Wessolowski U., 1990, Astron. Astrophys. 227, 171
Hamann W.-R., Dünnebeil G., Koesterke L., Schmutz W., Wessolowski U., 1991, Astron. Astrophys. 249, 443
Hamann W.-R., Leuenhagen U., Koesterke L., Wessolowski U., 1992, Astron. Astrophys. 255, 200
Harman R.J., Seaton M.H., 1966, Monthly Notices Roy. Astron. Soc. 132, 15
Heber U., Hunger K., Jonas G., Kudritzki R.P., 1984, Astron. Astrophys. 130, 119
Henize K.G., 1967, Astrophys. J. Suppl. 14, 125
Henize K.G., 1976, Astrophys. J. Suppl. 30, 491
Hiltner W., Schild R., 1966, Astrophys. J. 143,770
Houziaux L., 1968, Bull. Astr. Inst. Czechoslovakia 19, 265
Hu J.Y., Bibo E.A., 1990, Astron. Astrophys. 234, 435
van der Hucht K.A., Conti P.S., Lundstrøm I., Stenholm B., 1981, Space Science Review 28, 227
Iben I. jr., Kaler J.B., Truran J.W., Renzini A., 1983, Astrophys. J. 264, 605
Jeffery, C.S., 1995a, Astron. Astrophys. 297, 779
Jeffery, C.S., 1995b, Astron. Astrophys. 299, 135
Kaler J.B., Shaw R.A., Feibelman W.A., Lutz J.H., 1989, Astrophys. J. Suppl. 70, 213
Kawamura J., Masson C., 1995, Astrophys. J. (in press)
Köppen J., Tarafdar S., 1978, Astron. Astrophys. 69, 363
Koesterke L., Hamann W.-R., Wessolowski U., 1992a, Astron. Astrophys. 261, 535
Koesterke L., Hamann W.-R., Kosmol P., 1992b, Astron. Astrophys. 255, 490
Koesterke L., Hamann W.-R., 1995, in: White Dwarfs, Proc. of 9th European Workshop on White Dwarfs, D. Koester & K. Werner (eds.), Lecture Notes in Physics, Springer Verlag, p. 198
Kohoutek L., 1977, Astron. Astrophys. 59, 137
Lawson W.A., Jones A.F., 1995, in: Hydrogen–deficient stars, Proc. of 2nd International Colloquium on hydrogen–deficient stars, U. Heber & C.S. Jeffery (eds.), PASP Conference Series (in press)
Le Bertre T., Epchtein N., Gouiffes C., Heydari-Malayeri M., Perrier C., 1989, Astron. Astrophys. 225, 417
Leuenhagen U., Hamann W.-R., 1994, Astron. Astrophys. 283, 567 (Paper I)
Leuenhagen U., Heber U., Jeffery C.S., 1994, Astron. Astrophys. Suppl. 103, 445 (Paper II)
Masson C.R., 1989, Astrophys. J. 346, 243
Méndez R.H., Niëmela V.S., 1982, in: Wolf–Rayet Stars, Proc. IAU Symp. 99, C.W.H. de Loore & A.J. Willis (eds.), Reidel, Dordrecht, p. 457
Méndez R.H., Herrero A., Manchado A., Kudritzki R.P., 1991, Astron. Astrophys. 252, 265
Mihalas D., Kunasz P.B., Hummer D.G., 1975, Astrophys. J. 202, 465
Moore C.E., 1959, in: A Multiplet Table of Astrophysical Interest, NBS Technical Note 36
Moore C.E., 1970, NSRDS-NBS 3, Sect. 3
O'Dell C.R., Terzian Y., 1970, Astrophys. J. 160, 915
Paczyński B., 1970, Acta Astron. 20,47
Paddock G.F., 1915, Lick Obs. Bull. 9, 30
Pauldrach A., Puls J., Kudritzki R.P., Méndez R.H., Heap S.R., 1988, Astron. Astrophys. 207, 123
Perek L., Kohoutek L., 1967, Catalogue of Galactic Planetary Nebulae, Academia, Praha
Pettersson S.-G., 1982, Physica Scripta 26, 296
Pollacco D.L., Kilkenny D., Marang F., van Wyk F. Roberts G., 1992, Monthly Notices Roy. Astron. Soc. 256, 669
Pottasch S.R., Wesselius P.R., Wu C.-C., Fieten H., van Duinen R.J., 1978, Astron. Astrophys. 62, 95
Pottasch S.R., 1987, in: Planetary and Proto–Planetary Nebulae: from IRAS to ISO, Proc. of the Frascati workshop, Vulcano Island, A. Preite-Martinez (ed.), Reidel, Dordrecht, p. 1
Preite-Martinez A., Pottasch S.R., 1983, Astron. Astrophys. 126, 31
Preite-Martinez A., Acker A., Köppen J., Stenholm B., 1991, Astron. Astrophys. Suppl. 88, 121
Pwa T.H., Pottasch S.R., Mo J.E., 1986, Astron. Astrophys. 164, 184
Rao N.K., 1987, Q. J. Roy. Astron. Soc. 28, 261
Rao N.K., Giridhar S., Nandy K., 1990, Astron. Astrophys. 234, 410
Roche P.F., Allen D.A., Bailey J.A., 1986, Monthly Notices Roy. Astron. Soc. 220, 7P
Schmutz W., Hamann W.-R., Wessolowski U., 1989, Astron. Astrophys. 210, 236
Schönberner D., 1983, Astrophys. J. 272, 708
Schönberner D., 1986, in: Hydrogen Deficient Stars and Related Objects, K. Hunger, D. Schönberner & N. Kameswara Rao (eds.), D. Reidel Publishing Company, p. 221
Seaton M.J., 1979, Monthly Notices Roy. Astron. Soc. 187, 73P
Shaw R.A., Kaler J.B., 1985, Astrophys. J. 295, 537
Siebenmorgen R., Zijlstra A.A., Krügel E., 1994, Monthly Notices Roy. Astron. Soc. 271, 449
Smith L.F., Aller L.H., 1971, Astrophys. J. 164, 275
Tylenda R., Acker A., Stenholm B., Gleizes F., Raytchev B., 1991, Astron. Astrophys. Suppl. 89, 77
van der Veen W.E.C.J., Habing H.J., Geballe T.R., 1989, Astron. Astrophys. 226, 108
Webster B.L., Glass I.S., 1974, Monthly Notices Roy. Astron. Soc. 166, 491
Wenåker I., 1990, Physica Scripta Vol. 42, 667
Werner K., Heber U., Hunger K., 1991, Astron. Astrophys. 244, 437
Wessolowski U., Schmutz W., Hamann W.-R., 1988, Astron. Astrophys. 194, 160
Wood P.R., Faulkner D.J., 1986, Astrophys. J. 307, 659
Wright W.H., 1913, Publ. Lick Obs. 13, 196

This article was processed by the author using Springer-Verlag LaTeX A&A style file *L-AA* version 3.